Applied Acoustics 250 (2026) 111332

Contents lists available at ScienceDirect

Applied Acoustics

journal homepage: www.elsevier.com/locate/apacoust

Microstructural evolution and acoustic performance of heat-consolidated lightweight geopolymer granular panels

Nusrat Kabir [a], Tero Luukkonen [a,b], Johan Augusto Bocanegra [c], Davide Borelli [c], Priyadharshini Perumal [a,*]

[a] Fibre and Particle Engineering Research Unit, University of Oulu, Erkki Koiso-Kanttilan Katu, 90014 Oulu, Finland
[b] Department of Chemical Engineering Technology, University of Johannesburg, P.O Box 17011, Doornfontein 2088, South Africa
[c] Department of Mechanical, Energy, Management and Transportation Engineering, Università degli Studi di Genova, Via Opera Pia 15/A, 16145 Genova, Italy

ARTICLE INFO

Keywords:
Porous geopolymer material
Pore structure
Granular media
Dual porosity
Broadband acoustic absorption
Absorption coefficient

ABSTRACT

Achieving broadband sound absorption in lightweight materials requires understanding how pore morphology and tortuosity govern energy dissipation within porous networks. This study investigates the microstructural evolution and acoustic performance of heat-consolidated metakaolin-based geopolymer panels fabricated from foamed granules using hydrogen-peroxide to generate porosity. Panels are consolidated without external binders, resulting in lightweight structures with sufficient mechanical integrity for acoustic applications. Increasing foaming content promotes interconnected pore formation and tortuosity, transforming the structure from discrete intergranular voids into a continuous porous network. Microstructural analysis confirms the coexistence of intergranular and intragranular porosity, with a hierarchical pore structure spanning nanometer to millimeter scales and open porosity ranging 25–40%. Across the investigated compositions, these microstructural variations are associated with a transition from localized resonance-dominated absorption toward broadband dissipation, as observed in normal-incidence acoustic measurements over 200–4300 Hz, with absorption coefficients reaching 0.8–0.9 for panels prepared with foaming levels 4–5 wt% hydrogen-peroxide. The geopolymer panels exhibit acoustic performance comparable to conventional polyurethane and melamine foams while providing mechanical strength at the MPa scale (up to $\sim$ 4 MPa), compared to the kPa-level strength of polymer-based absorbers. Unlike the highly elastic nature of polymeric materials, the geopolymer panels possess a rigid structural response, making them suitable for applications requiring both sound absorption and mechanical stability. Overall, the results show that granular geopolymer systems consolidated without any external binders provide a viable pathway for achieving broadband acoustic performance while maintaining mechanical integrity and providing a proof-of-concept for manufacturing methodology.

1. Introduction

Noise pollution is an increasingly prevalent environmental concern, driven by rapid urbanization and increased human activity associated with rising living standards [1]. Common sources include transportation systems, industrial operations, and indoor sources such as home appliances, entertainment systems, and HVAC (Heating, Ventilation, and Air Conditioning) equipment, particularly in densely populated urban environments. Noise pollution negatively impacts ecology and human health, impairing physical and mental performance [2], especially in schools [3]. Excessive exposure can cause hearing loss [4], cardiovascular dysfunction [5], mental health disorders [6], and annoyance, fatigue, sleep disturbances, and sound sensitivity [7,8]. In indoor and building environments, improving acoustic comfort, particularly through the control of airborne noise, has therefore become an important design requirement. Sound-absorbing materials are widely used to control airborne noise by dissipating acoustic energy and reducing sound reflections within enclosed spaces [9]. A range of porous materials, such as mineral wool, glass wool, fiberglass, and polymeric foams like polystyrene and polyurethane, have been traditionally used for acoustic applications due to their high sound absorption efficiency [10–15]. Nevertheless, these materials are synthetically produced from nonrenewable petrochemical sources and raise concerns related to recyclability, end-of-life management, and potential health risks

* Corresponding author.
E-mail address: priyadharshini.perumal@oulu.fi (P. Perumal).

https://doi.org/10.1016/j.apacoust.2026.111332
Received 24 November 2025; Received in revised form 22 February 2026; Accepted 6 April 2026
Available online 12 April 2026

associated with fibrous particulates [16,17]. In response to this, granular-based absorbers have attracted increasing attention, as they are often derived from natural aggregates, recycled materials, or industrial by-products and offer flexible microstructural design for tailoring acoustic performance [10,18,19].

Lightweight granular materials (LGMs) composed of loosely bound or unconsolidated particles with irregular or spherical morphology, exhibit porosity and low density, making them attractive for acoustic applications [20–22]. When incorporated into consolidated granular structures, LGMs combine low mass with improved mechanical integrity, together with favorable physicochemical properties such as low thermal conductivity and refractory behavior [10]. Unconsolidated granular beds typically require external confinement, whereas consolidation enables mechanically coherent, self-supporting porous elements suitable for practical acoustic applications while preserving interconnected porosity for sound absorption [10,18]. LGMs effectively dissipate sound through internal air voids and airflow resistance through their porous structure. Their acoustic response can be influenced by particle interactions with packing conditions, and boundary constraints, making granular systems attractive for tunable sound absorption [20]. Several studies have reported that granular-based acoustic materials can achieve effective sound absorption, including arlite, perlite, vermiculite [10], rubber granules [23,24], and expanded clay [25,26]. These materials have demonstrated a combination of acoustic functionality and adequate mechanical performance for building-related applications. However, they are commonly used in loose form and therefore require external binders to achieve structural integrity, which can increase material consumption and processing complexity. Binders reported in the literature include epoxy resin [25], polyurethane [27], or fly ash and cement [26], and some fabrication routes remain energy-intensive due to extended curing at elevated temperatures [28,29]. These limitations highlight the need for consolidated granular systems that can achieve mechanical coherence while minimizing additional binders and processing complexity.

Geopolymers are considered as a green binder [30] and potentially sustainable alternatives for building materials [31,32]. Geopolymers are aluminosilicates with a three-dimensional structure and sometimes considered a subclass of alkali-activated materials [33]. Their preparation involves alkali solutions mixed with amorphous aluminosilicate materials (such as fly ash, metakaolin, and blast furnace slag) at (near) room temperature [34]. When blowing agents (e.g., H_2O_2, Al^0, or Si^0) are added under alkaline conditions, gas bubbles form, creating a porous structure and expansion [35]. Yu et al. [36] prepared geopolymer granules based on metakaolin and solid sodium metasilicate, utilizing varying concentrations of H_2O_2, which demonstrated open porosity of 72% with 20% H_2O_2. The development of porosity within these materials is crucial, as the acoustic performance of porous materials is closely linked to pore structure characteristics such as porosity, pore size, and tortuosity [10,37–39]. While increased open porosity can promote sound absorption, as reported by Leiva et al. [37], demonstrating enhanced acoustic performance of porous geopolymers over the frequency range 100–5000 Hz, they also stated that excessively high open porosity may reduce pore-wall interactions and diminish absorption efficiency. These observations highlight that sound absorption is frequency dependent and governed by the combined morphology and connectivity of the pore network [39]. Porous materials act as acoustic absorbers by trapping incident sound waves and dissipating acoustic energy through viscous and thermal losses at the pore walls [39]. Although several studies have established empirical relationships between pore characteristics and sound absorption efficiency in granular media [23,26,38], most focus on loose beds or pre-formed granules with largely predefined pore structures. The role of pore features evolving during material processing and consolidation in governing the acoustic behavior of granular systems therefore remains insufficiently understood and so requires further experimental investigation based on controlled material processing, microstructural observation, and comparative analysis of the resulting acoustic behavior.

The acoustic behavior of porous media can be described by impedance-based models such as the Johnson-Champoux-Allard (JCA) model, which relates sound absorption to microstructural parameters including porosity, airflow resistivity, tortuosity, and viscous and thermal characteristic lengths [40]. Although JCA model is formulated for idealized pore structures and its applicability to irregular or hierarchical granular network is limited, it is referenced here to contextualize the role of pore morphology and microstructural parameters in acoustic dissipation, rather than for quantitative implementation. In such systems, viscous and thermal boundary layer effects govern sound energy dissipation within interconnected pores, with the characteristic lengths reflecting pore geometry and shape. While small and tortuous pores enhance high-frequency absorption through viscous-thermal losses, larger and more connected pores favor low-frequency attenuation [10,37]. Arenas et al. [39] demonstrated that porous geopolymer composites containing crushed granite and construction and demolition waste exhibit a strong correlation with acoustic characteristics and sound absorption properties. The effectiveness of sound absorption in geopolymers is influenced by key microstructural factors such as porosity, pore size, tortuosity, and the permeability of the pore network have a close relationship with acoustic characteristics and sound absorption. Wallah [41] reported that geopolymers have notable sound absorption capacity combined with minimal shrinkage, which helps maintain their porous structure, durability, and long-term acoustic performance. Raja et al. [42] showed that the sound absorption behavior of geopolymer panel manufactured from fly ash had an absorption coefficient (α) between 0.2–0.35 in the frequency range of 1200 Hz to 6300 Hz. Using fly ash and aluminum waste, Leiva et al. [37] created porous geopolymer composites with an approximate 14–21% open porosity, achieving sound absorption coefficients between 0.3 and 0.5 over a broad frequency range of 250–5000 Hz. Acoustic dissipation in porous granular media is associated with factors such as airflow resistivity, visco-inertial coupling, and, in consolidated systems, frame-related effects, which are closely related to the pathways formed within the pore structure. Achieving efficient sound absorption at lower frequencies is generally challenging in porous geopolymer systems, with pore size and pore morphology being important contributing factors. Accordingly, this study focuses on the development of heat-consolidated granular geopolymer materials and the experimental observation of how the evolution of pore morphology affects frequency-dependent sound absorption.

Geopolymer granules have potential for porous consolidated structures incorporating porosity at two levels: intrinsic microporosity and macroporosity caused by foaming. This dual porosity is expected to enhance acoustic absorption by increasing internal surface area and dissipative pathways for sound waves [43]. Although granular materials and geopolymer composites individually exhibit promising acoustic properties, no studies have systematically combined these approaches to produce fully consolidated porous panels without additional binders. The influence of dual porosity and pore structure on the acoustic performance of such consolidated systems remains poorly understood. The concept of developing the granules involves an integrated process combining granulation, alkali activation, and direct foaming [36]. Their formation was driven by adhesive, cohesive, and interfacial forces [43,44], while subsequent geopolymerization during curing yielded a durable, porous aluminosilicate network [45,46]. Developing heat-consolidated granular media can simplify manufacturing processes, reduce material complexity, and improve mechanical integrity while preserving acoustic efficiency. Heat consolidation refers to the process by which discrete particles or granules are thermally bonded into a solid, cohesive structure without the application of external mechanical pressure. This method eliminates the need for additional binders or compaction. The granular geopolymer media developed through this approach offer targeted sound absorption across specific frequency ranges, enhanced durability against moisture and mechanical stress, and suitable versatility for diverse architectural applications. Furthermore, their production often incorporates recycled materials, promoting environmental sustainability and aligning with increasing regulatory and market demands.

While this study uses metakaolin and Na-metasilicate to develop geopolymer-based granular acoustic panels, the approach also serves as a proof-of-concept for adapting similar methods to other raw materials, including industrial byproducts such as silica and alumina-rich waste such as mining residues and bottom ash [47,48] could be valorized into acoustic materials through comparable foaming and heat consolidation strategies. This work demonstrates the potential to optimize pore structures to enhance acoustic performance in alkali-activated porous systems while supporting circular economic efforts by converting low-value waste into functional acoustic products. Therefore, the objectives of this study are to i) develop heat-consolidated, geopolymer-based porous granular panels without external binders; ii) optimize the concentration of the granulation fluid to modulate pore structure and acoustic performance; and iii) interpret, observe and establish the effect of pore structure characteristics on frequency-dependent sound absorption and mechanical strength. Although aspects of the relationship between pore structure and acoustic performance have been explored in previous studies on loose granular media, pre-formed granules, or architected acoustic structures, their applicability to granular systems formed through material processing and heat consolidation remains insufficiently examined. The present study therefore addresses the following research questions: i) How does the concentration of the foaming agent (H_2O_2) influence pore structure and acoustic absorption performance? ii) How porous microstructures evolve, including size distribution and connectivity, influence the selective absorption of sound across different frequency ranges? iii) How does the acoustic performance of the developed panels compare with conventional absorbers? By addressing the link between pore structure and acoustic performance, this work would provide valuable insights into designing external binder-free materials for acoustic applications. The present study focuses on material development and acoustic performance, while practical aspects relevant to building applications such as fire resistance, moisture durability, freeze–thaw resistance, and installation considerations remain important for assessing their broader applicability.

2. Materials and methods

2.1. Fabrication of porous granules and acoustic panels

Metakaolin was used as the aluminosilicate precursor (MK, MetaMax, BASF, USA). The chemical composition of MK is shown in Table 1 (as determined by X-ray fluorescence using a PanAnalytical Minipal 4 instrument). As an alkali activator, solid anhydrous sodium metasilicate (composition: Na_2O 50.8 wt%, SiO_2 46.7 wt%, and H_2O 2.5 wt%) supplied by VWR Alfa Aesar (Germany) was used. The activator and precursor were mixed at a mass ratio of 0.53 (molar ratio of $SiO_2/Na_2O = 2$, $Na_2O/Al_2O_3 = 1.5$, and $SiO_2/Al_2O_3 = 3$, following preliminary optimization for stable geopolymerization with ratios of 1.2, 1.5, and 2 for SiO_2/Na_2O). The blended powder was homogenized in a ball mill (Germatec, Germany) for 1.5 h, resulting in an average particle size of 6.7 μm and true density of 2.6 g/cm^3.

Table 1
Chemical composition (%) of MK expressed as oxides.

Oxides	Amount (%)
Al_2O_3	29.50
SiO_2	35.40
Na_2O	0.36
CaO	0.06
TiO_2	1.57
Fe_2O_3	0.41

Granules were prepared in a high-shear mixer (Eirich EL1) using aqueous 1–10 wt% H_2O_2 solutions (diluted from 30 wt% hydrogen peroxide, VWR, Belgium) as both the granulation fluid and foaming agent. Under alkaline conditions, H_2O_2 decomposes to release O_2 gas ($2H_2O_2 \rightarrow 2\ H_2O + O_2\uparrow$), and the resulting bubbles form pores. The amount of H_2O_2 therefore controls the intensity of gas evolution, bubble growth, and foaming during granulation. At low concentrations (≈ 1–2%), limited gas release forms fine intragranular pores, whereas higher concentrations promote coalescence and partial expansion of the granules.

Mixing in the high-shear mixer was performed at 1200 rpm (impeller speed) and 170 rpm (pan rotation speed) with a 30° tilt angle· H_2O_2 was dosed dropwise to the blended powder during a mixing period of approximately 20 min, corresponding to an average liquid-to-solid ratio of ~ 1:3. The selected dosing level was kept below conditions known to induce bulk agglomeration. Foaming and granulation under these conditions resulted in the formation of granules that remained structurally stable, without significant coalescence or collapse· H_2O_2 decomposition was initiated during granulation at ambient laboratory temperature using the same alkaline condition (pH > 12) and raw materials for all samples and could continue during the subsequent thermal curing step. Therefore, temperature, pH, and impurity levels during granulation were consistent across all samples. One reference batch (G-R) was prepared using deionized (DI) water. After the granulation process, freshly prepared granules were sieved into a diameter to obtain a size range of 2–8 mm. The granule size range was selected during material development to achieve favorable packing density, based on previous study showing that mixed-size granular distributions allow smaller particles to fill the voids between larger ones [49]. This packing configuration promotes intergranular contact and bonding during expansion and curing for the acoustic investigations presented in this study. The sieved granules were placed in a plastic bag and kept at 60 °C for 4 h and preserved in separate plastic containers at room temperature (22 °C) until used.

To produce the consolidated acoustic panels, freshly prepared 2–8 mm granules were immediately transferred into cylindrical silicone molds (internal diameter 45 mm, thickness 50 mm) to ensure random packing without orientation. This size range provided effective particle interlocking and air-void distribution while maintaining structural stability during foaming. Each packed mold was lightly compacted to eliminate large voids and sprayed with a thin layer (~1 mL) of aqueous H_2O_2 solution matching the granule batch concentration to promote surface bonding and open-pore connectivity at particle interfaces. The sealed molds were then subjected to thermal consolidation at 60 °C for 4 h, followed by curing at room temperature (22 °C) for 24 h. Curing parameters were optimized through exploratory trials: H_2O_2 dosages exceeding 5% led to excessive foaming and loss of the granular structure, so 1–5 wt% solutions were selected for subsequent panel development (Fig. S1 in supplementary material). The temperature and duration were chosen as the minimum conditions enabling sufficient surface geopolymerization and neck formation between granules without causing dehydration cracking or bubble collapse. At low temperature (< 22 °C) or shorter durations (< 4h), incomplete consolidation and weak intergranular bonding were observed (Fig. S2 in the supplementary material).

During heating, residual H_2O_2 and moisture released additional oxygen, enhancing microporosity near particle contacts as the geopolymeric gel hardened into a cohesive network of bonded granules. Consolidation was confirmed by stable geometry, absence of surface cracking or granule detachment, and continuous bonding between particles observed under microscopy [25,26,49]. After heat treatment, the panels were cooled and cured at room temperature for 24 h and later they were demolded and preserved in a plastic container until used. The experimental design is illustrated in Fig. 1, while a representative sample image is shown in Fig. 2. All samples were prepared at laboratory scale using the same equipment, formulation, and processing parameters

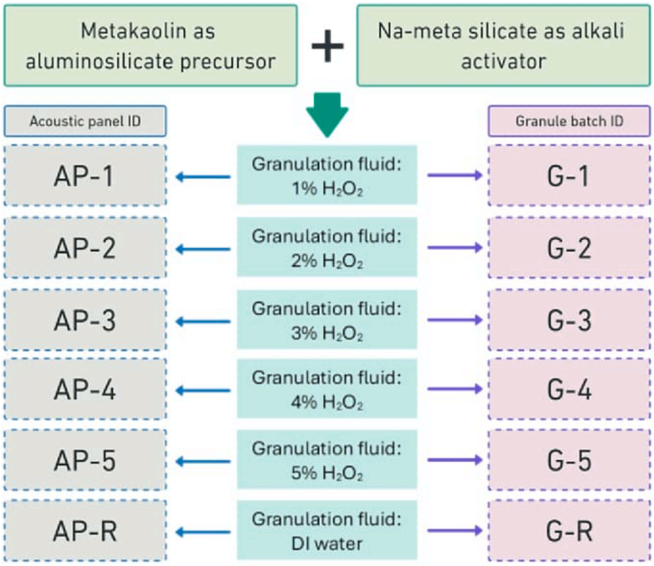

Fig. 1. Sample ID for the porous granules and granular media preparation. The abbreviations used for different batches are shown in the figure (in the abbreviations, AP = acoustic panel or G = granules, the concentration in the granulation fluid of H_2O_2 is indicated by the number associated with the IDs).

to ensure consistent material fabrication. A systematic analysis of scale-up behavior and batch-to-batch variability was beyond the scope of the present study.

2.2. Characterization of granules and acoustic panels

2.2.1. Density and porosity measurement

The true density (D_T) of the loose granules and the acoustic panels was determined by using a helium gas pycnometer (Micrometrics, AccuPyc II 1340, unit 1 SN1296) using approximately 2 g of each sample. 10 measurements were taken for each sample type. Apparent density (D_A) and open porosity were determined according to EN 1936:2006 [50] using the Archimedes method for acoustic panels. Total Porosity (P%) was determined using the following Eq. (1). closed porosity was obtained as the difference between total and open porosity.

$$P\% = \left[\frac{(D_T\text{-}D_A)}{D_T}\right]*100 \tag{1}$$

Bulk density (ρ) is measured by the following Eq. (2) in unit, g/cm^3. 6 samples were measured for each batch.

$$\rho = \frac{\text{Mass of acoustic panel}}{\text{Total volume}} \tag{2}$$

Total volume (V) of the samples was measured by the following equation (3).

$$V = \frac{\pi}{4} d^2 h \tag{3}$$

where d and h are the diameter and height of the sample, respectively.

2.2.2. Specific surface area and nanometer-scale porosity

The specific surface area of the loose granules and consolidated acoustic panels were measured using a Micromeritics ASAP 2020 equipment. Measurements were carried out based on nitrogen (N_2) adsorption–desorption isotherms at liquid nitrogen temperature (−196 °C). The Brunauer-Emmett-Teller (BET) method was used to determine the specific surface area, while the Barrett-Joyner-Halenda (BJH) model was applied to analyze pore size distribution and pore volume using the desorption data. The BET method effectively captures contributions from micropores (< 2 nm) and mesopores (2–50 nm) [51,52].

However, both BET and BJH techniques are limited in their ability to detect macropores (> 50 nm) [53], which are commonly formed in porous materials produced with chemical blowing agents such as hydrogen peroxide (H_2O_2) as incorporated in this study. As a result, the measured surface area and pore volume may underestimate the total porosity, particularly in samples containing larger pores. These methodological limitations were considered during the result interpretations. Accordingly, the BET analysis was primarily used to confirm the presence and evolution of nanometer-scale porosity in response to increasing H_2O_2 concentration, rather than to characterize the macroporous structure governing sound absorption. Optical microscopy (Section 2.2.3) and scanning electron microscopy (SEM) (Section 2.2.4) were employed to characterize larger pores and evaluate the evolution porosity in consolidated panels. This combined approach enabled multi-scale assessment of pore formation (from nanometers to millimeters scale) and supports an integrated interpretation of how hierarchical pore structure develops with H_2O_2 concentration.

2.2.3. Optical microscopy image analysis

The X-Y cross-sectional (shown in Fig. 2) surfaces of the acoustic samples were examined using a Leica MZ6 optical microscope equipped with a DFC420 camera. Images were acquired in TIFF format, with pore regions segmented as shown in Fig. 3 (left). The files were studied in ImageJ-win64 (v 1.54P) to classify the pore size, pore area as well as the frequency of the pores. For each sample, 3 images were analyzed. All the images were binarized using same automatic thresholding option in

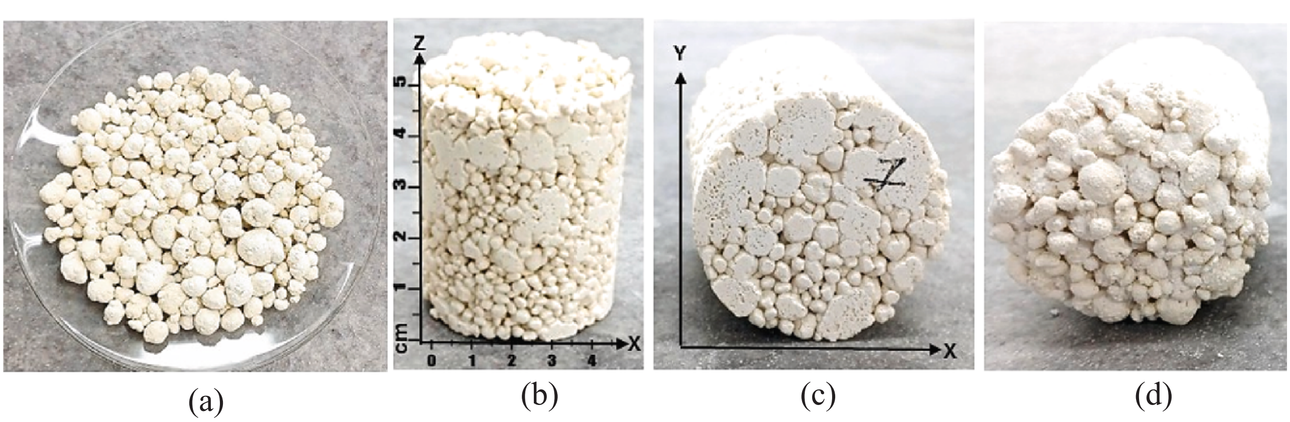

Fig. 2. (a) 2–8 mm loose granules; Sample image of the consolidated acoustic panel: (b) full panel; (c) bottom surface; and (d) top surface. The coordinates shown in the figure are used to describe the sample orientation in the image analyses.

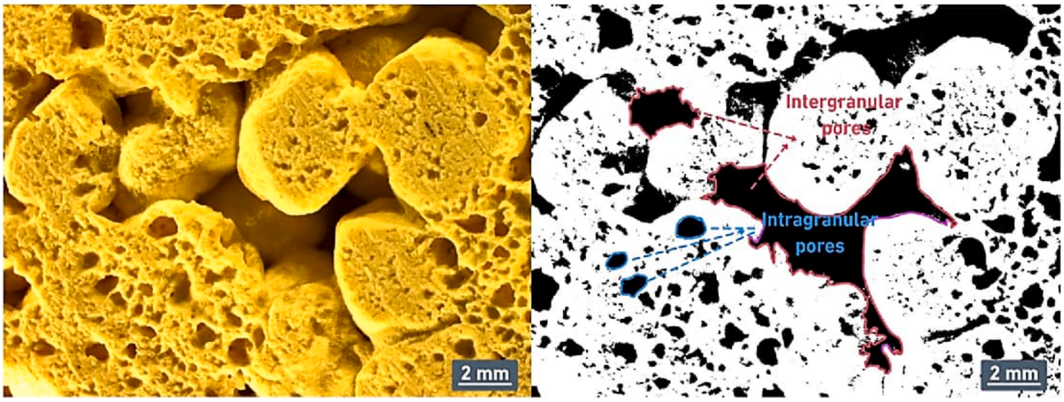

Fig. 3. Illustrative optical images used for pore structure analysis: original image (left) and processed image (right). In the processed image, black regions indicate pores, while white regions correspond to the solid matrix.

ImageJ for all samples, where black areas denote pores and white areas represent the geopolymer matrix in Fig. 3 (right). This image analysis provided an evaluation of surface pore distribution and intergranular void size in the X-Y plane to support understanding of how foaming behavior influences airflow pathways and acoustic response. Pore features were expressed as percentage (%) and averaged over multiple cross-sectional images. Optical microscopy represents a local two-dimensional (2D) surface observation of pore morphology in the micrometer to millimeter range, which is relevant to airflow pathways and to the acoustic behavior in the studied frequency range. These 2D statistics are therefore used to illustrate relative pore-size ranges and comparative trends between samples rather than to provide bulk volumetric measurements.

2.2.4. Scanning electron microscopy (SEM)

For all the acoustic panels, surface morphology was studied for X-Z cross sections (shown in Fig. 2) at 250 × magnification using a field-emission scanning electron microscope fitted with an energy dispersive X-ray spectrometer (FE-SEM-EDS, a Zeiss Ultra plus instrument). For each batch, three samples were imaged. Prior to analysis, the cross-sections were revealed by casting the samples in epoxy resin (Buehler, Epoxicure) and polishing them with SiC grinding paper (Buehler Grit P240, P600, and P1200) using ethanol flushing. The samples were coated with carbon before SEM analysis. Epoxy mounting served only for mechanical support during preparation, and pore features were assessed in the interior cross-section rather than the external surface. Any potential resin infiltration is expected to be limited, and the nanometer-thin carbon coating does not affect the micrometer-scale pore morphology reported here. SEM was used for qualitative visualization of the transition in pore morphology and connectivity with granulation fluid concentration in the X-Z plane at the micrometer scale as well as to observe the bonding quality between granules and to verify the presence of open-pore connections and airflow pathways that influence viscous dissipation in the X-Z plane, corresponding to the sound propagation direction.

2.2.5. X-ray computed microtomography (XCT)

Three (X-Z cross sections in Fig. 2) of the acoustic panels (AP-1, AP-3-AP-5) were imaged using a GE *Phoenix* V|tome|x X-ray computed microtomography device. The scans were conducted using an accelerating voltage of 100 kV and a tube current of 280 μA, resulting in a total power output of 28 W. A 0.1 mm copper (Cu) filter was applied to reduce beam hardening effects. All samples were imaged using helical scanning mode, in which the sample rotated while simultaneously moving vertically. The total vertical travel ranged from 91.68 to 92.00 mm, with 3666 to 3918 angular steps acquired per scan. Each step corresponded to an angular increment of 0.18°, leading to a total rotation of 651.8° to 696.7°. At every step, the detector captured three exposures, each with an exposure time of 333 ms, and averaged them to enhance image quality. As a result, total scan durations ranged from 96 to 101 min. During reconstruction, a beam hardening correction coefficient of 8 (on a scale of 0–10) was applied, and the final voxel size of the reconstructed volume was 25.02 μm. Micro-CT enabled three-dimensional (3D) visualization of internal structure of representative samples and quantification of porosity (3D), and tortuosity, parameters directly linked to airflow resistivity and acoustic absorption. Although vertical gradients layered along the foaming/curing direction are observed in the XCT images, they were used in this work to qualitatively represent pore connectivity along the sound propagation direction, in line with the objectives of this study.

Porosity values are compared only within the same measurement technique. Archimedes measurements are used for quantitative comparison among samples. Optical microscopy and X-ray computed tomography are employed to qualitatively assess pore morphology and connectivity in different planes. Optical microscopy reflects surface porosity in the X-Y plane, while XCT provides internal structural information in the X-Z plane, aligned with the sound propagation direction. The voxel size (≈ 25 μm) enables characterization of pore connectivity and structural features at a scale relevant to airflow pathways and acoustic behaviour in the studied frequency range.

2.2.6. Tortuosity

$$\tau_{avg} = \frac{1}{n}\sum_{i=1}^{n}\frac{\text{Branch length}_i}{\text{Euclidean distance}_i} \qquad (4)$$

Tortuosity was used as a representative descriptor of pore connectivity in this study, given its relevance to transport-related behavior and compatibility with the available imaging resolution. It was determined using ImageJ-win64 (v 1.54P, Fiji distribution) based on 3D X-ray microtomography images. The image stacks were first preprocessed by applying Gaussian filtering to reduce noise, followed by thresholding to segment the pores and solid phases. The binarized images were then skeletonized using the Skeletonize3D plugin and the resulting skeletons were analyzed with the Analyze Skeleton (2D/3D) plugin to quantify path lengths in Fig. 4 (right). Skeleton-based tortuosity captures geometric path complexity and pore connectivity, which are relevant to sound propagation, but does not explicitly account for pore throat constrictions which dominate viscous loss.

Tortuosity was calculated as the ratio of the branch length (pixel) and Euclidean distance (pixel) for each branch. The average Tortuosity (τ_{avg}) of the samples was determined from the following equation (4). Tortuosity analysis was performed on representative samples (AP-1, AP-3, and AP-5) to illustrate the evolution of pore connectivity trends across the H_2O_2 concentration range. The results were later compared with the

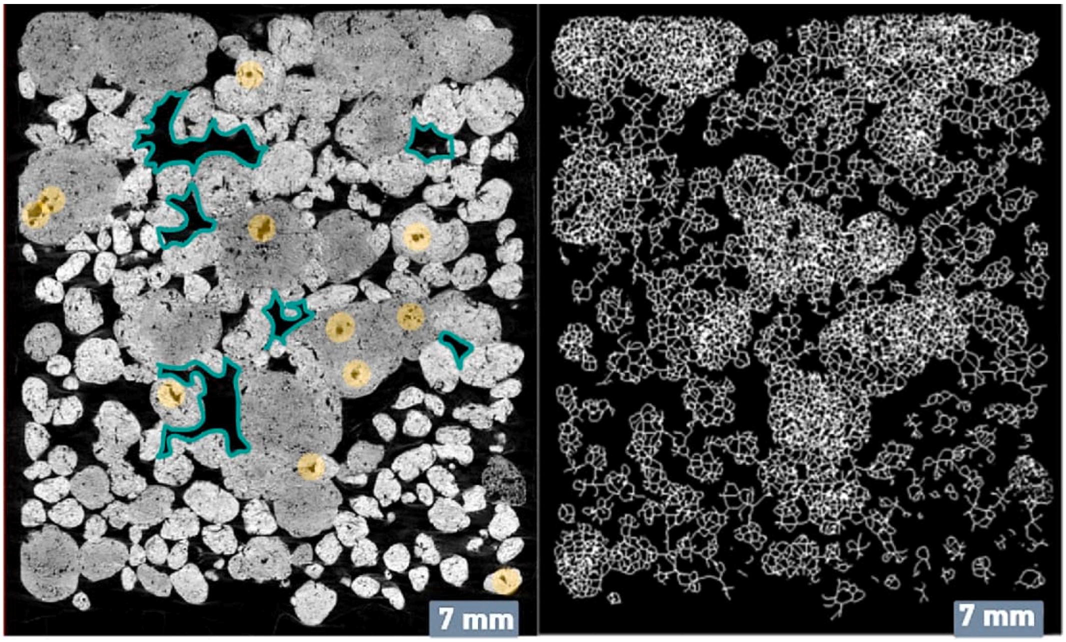

Fig. 4. Illustrative X-ray microtomography image of acoustic panel (left), showing examples of intra-granular pores (yellow) and inter-granular pores (green). The processed skeletonized image (right) is used for tortuosity analysis.

sound absorption results to interpret how pore connectivity and path complexity influence viscous and thermal losses across frequency bands.

2.2.7. *Mechanical properties*

Both the flexure and compression tests were performed to measure the mechanical properties of the acoustic panels using a Zwick/Roell Z100 testing machine. Young's modulus and the stress at maximum load break were measured. A 1 kN load cell was used for the flexural test and compression tests at 1 mm/min rate until breakage.

80 × 20 × 20 mm specimens were used to carry out both the flexural tests (by means of a three-point loading system) and compression test, following the procedures described by [26]. Six tests were carried out for each specimen to determine the average mechanical properties. Statistical differences among groups were evaluated using one-way analysis of variance (ANOVA) with a significance level of 0.05. The mechanical results are presented to evaluate the structural integrity and behavior of the panels resulting from the material processing and to support the demonstration of the consolidation approach for granular acoustic materials. Environmental effects, such as moisture-conditioned mechanical performance, were beyond the scope of the present study. Mechanical strength data were later correlated with porosity and intergranular bonding features to evaluate the structural integrity.

2.2.8. *Acoustic test method*

The normal incidence sound absorption coefficient (hereafter referred to as α) was measured using a Kundt's tube system (Materiacustica) equipped with three precision microphones (Fig. 5b) (PCB Piezotronics 378C10) and a data acquisition unit (NI USB-4431) (Fig. 5a), following ISO 10534–2 [54] and the extended three-microphone method. Although ISO 10534–2 defines a two-

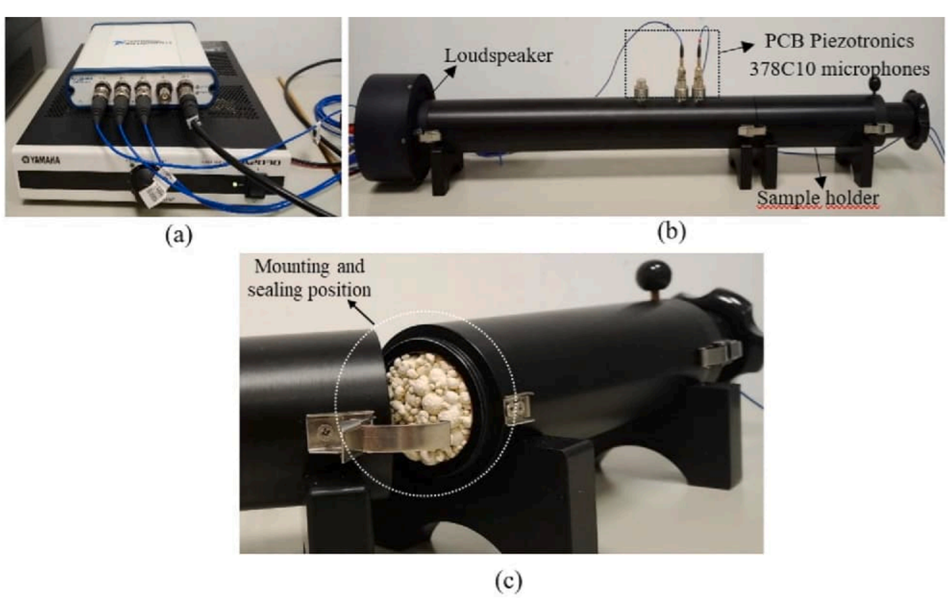

Fig. 5. (a) Data acquisition unit (NI USB-4431), (b) The complete impedance tube, (c) The sample holder with rigid backing.

microphone transfer-function method, an extended three-microphone configuration was used here to improve measurement accuracy. The additional microphone enables simultaneous estimation of sound pressure and particle velocity, reducing phase and standing-wave errors at higher frequencies. The setup included a rigid cylindrical tube (Fig. 5a) (45 mm diameter) designed for plane wave propagation in the 200–4300 Hz frequency range. All acoustic panels (AP-R to AP-5) were tested at their as-cast thickness of 50 mm. Each sample was placed at the tube's end against a rigid backing (Fig. 5c), while a chirp signal was generated by a loudspeaker at the opposite end. A chirp signal was used because it provides a high signal-to-noise ratio under linear measurement conditions in accordance with ISO 10534–2. Due to surface asymmetry, measurements were initially performed for both sample orientations; the smoother bottom face showed lower absorption; therefore, all reported results correspond to the top-surface orientation. Three flush-mounted microphones at known positions enabled simultaneous capture of transfer functions. The three-microphone method allowed for accurate estimation of the complex reflection coefficient and sound absorption coefficient by taking into account both pressure and particle velocity. This method improves measurement reliability, especially where two-microphone techniques are prone to phase errors and standing waves. Calibration was performed using a reference sample, with corrections applied for phase mismatch and tube losses. Six specimens for each batch were tested under identical environmental conditions at room temperature to ensure repeatability, variation and accuracy. To ensure measurement consistency, each specimen was carefully mounted with tight sealing in the impedance tube.

From the measurements, a widening of the min–max range at higher frequencies was observed (Fig. 15), which reflects the intrinsic properties of the granular composite. Granular and porous materials exhibit broad and complex sound absorption due to their heterogeneous structures and multi-scale acoustic interactions [43]. However, this heterogeneity also complicates sound propagation measurements, as demonstrated by Owens and Daniels, who also showed that acoustic transmission in granular media depends on particle-scale contact networks; although the present materials differ from granular chains, this concept supports the interpretation that pore connectivity influences macroscopic acoustic behavior in heterogeneous porous granular media [55]. At higher frequencies, where wavelengths are smaller than pore or grain sizes, absorption increases via viscous friction, thermal losses, and scattering within the material's microstructure [40]. The random distribution of particles and voids generates multiple scattering and local impedance fluctuations, which enhance viscous and thermal dissipation and thereby broaden the effective absorption bandwidth [56]. This wideband absorption is both expected and beneficial for acoustic applications [57]. To compare the results further, the mean values (represented by dotted lines) were considered in section 3.4. The obtained absorption data were analyzed in conjunction with pore structural parameters to identify how microstructural changes influenced the acoustic response at different frequencies in section 4.

3. Results

While the following sections first present the structural and morphological characteristics of the developed materials, the primary objective of this study is to assess their sound absorption performance. Accordingly, the acoustic properties will be discussed in detail after presenting the material characteristics.

3.1. True density and porosity measurement

The density of the milled raw material comprising MK and Na-metasilicate was 2.6 g/cm^3. The true density of the individual granules (G-1 to G-5, G-R) was 1.8–2.1 g/cm^3, indicating that the addition of H_2O_2 or DI water reduced the density by approximately 30% compared to raw materials. Similarly, the true density of the acoustic panels (AP-1 to AP-5, AP-R) remained within 2.01–2.1 g/cm^3, suggesting the consolidation process had no significant impact on the overall density. The bulk density of the panels (Table 2) decreased with increasing H_2O_2 content, reflecting the effect of peroxide-induced foaming. Compared to the reference sample AP-R, AP-1 showed a 16% reduction, indicating a significant decrease even at 1 wt% H_2O_2. Samples AP-2 to AP-4 exhibited a 25–37% reduction, suggesting the decrease became less pronounced with moderate peroxide levels. At 5 wt% H_2O_2 (AP-5), the density dropped, marking a 41% reduction compared to AP-R. These findings confirm that H_2O_2 effectively induces porosity, resulting in lightweight structures. Such structures are known to be suitable for acoustic applications [58].

Porosity analysis (Fig. 6) showed that the total porosity in acoustic panel batches (AP-1 to AP-5) changed in a narrow range, with an initial 50% increase at 1 wt% H_2O_2 compared to the reference prepared with DI water (AP-R). Increasing H_2O_2 beyond this did not significantly raise total porosity but shifted pore structure from closed pores to more open pores, enhancing connectivity and bonding. This transition indicates a pore connectivity threshold between approximately 2 and 3 wt% H_2O_2, as inferred from qualitative analysis from Fig. 6, where isolated or closed pores progressively evolve into a continuous open pore network. This indicates that further increases in H_2O_2 content concentration led to only modest increases in total volumetric porosity, while pore structural evolution becomes the dominant effect. Similar trends have been reported in literature. Alves et al. [59] found that beyond a saturation threshold (0.6 wt% H_2O_2 solution), porosity remained constant (50%) in lightweight geopolymer panels (prepared with metakaolin, sodium silicate, sodium hydroxide, and hydrogen peroxide), possibly due to the matrix's limited capacity to accommodate more gas bubbles. Likewise, Kim et al. [19] observed that although H_2O_2 improved pore uniformity and increased porosity, adding it beyond 10 wt% H_2O_2 solution caused pore coalescence and foam collapse, thereby limiting further enhancement in porosity (maximum 54%) within the geopolymer matrix prepared with metakaolin and sodium dodecyl sulfate. Prior studies have reported diverse density-porosity characteristics in acoustic absorber systems. Fly ash-based geopolymer incorporating aluminum waste, for example, has shown bulk densities in the range of 0.9–1.2 g/cm^3 with open porosities between 11% and 21% [37]. In another case, epoxy-resin-bound expanded clay aggregates demonstrated a significantly lower bulk density of 0.45 g/cm^3 alongside a total porosity of 55% [25]. The geopolymer granular panels developed in this present study offer a notable advancement, achieving open porosities of 23–40% while maintaining bulk densities approximately 30–40% lower than those reported by Leiva et al. [37] and comparable to the values observed in the epoxy-based system, yet with enhanced total porosity. These comparisons serve to contextualize performance relative to geopolymer-based panels and granular acoustic media, acknowledging that direct quantitative equivalence is limited by differences in material chemistry and processing.

3.2. Pore structure analysis

Table 3 presents the specific surface area values of the granules and their corresponding consolidated acoustic panels. The objective was to assess how increasing H_2O_2 concentration influences surface area and

Table 2
Bulk density of the acoustic panels.

Batch ID	Bulk density, g/cm^3
AP-R	1.00
AP-1	0.84
AP-2	0.75
AP-3	0.68
AP-4	0.63
AP-5	0.59

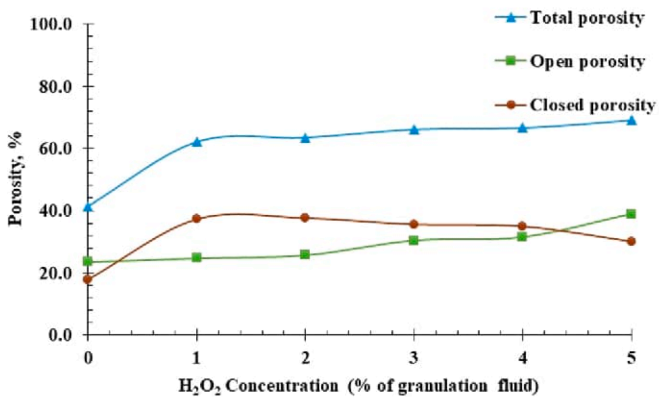

Fig. 6. Porosity of acoustic panels.

Table 3
Specific surface area of the granules and acoustic panels.

Batch ID	Specific surface area, m^2/g	Batch ID	Specific surface area, m^2/g
G-R	4.0	AP-R	4.0
G-1	0.3	AP-1	0.4
G-2	0.26	AP-2	0.44
G-3	0.2	AP-3	0.5
G-4	0.46	AP-4	0.66
G-5	0.6	AP-5	1.0

nanometer-scale porosity. Reference samples without H_2O_2 (G-R and AP-R) exhibited the highest specific surface areas, likely due to the dense and uniform microstructures formed during geopolymerization without foaming agents.

In H_2O_2-treated samples, the surface area varied with concentration. A general increasing trend was observed in the acoustic panels from AP-1 to AP-5 (0.4 to 1.0 m^2/g), reflecting the role of gas evolution in creating finer, interconnected pore networks. This interpretation is supported by the findings of Gonzalez et al. [60], who investigated the role of gas evolution in pore formation during the synthesis of porous carbon materials using 30 wt% H_2O_2 as blowing agent. Compared to their granule counterparts (e.g., AP-5 = 1.0 m^2/g vs. G-5 = 0.6 m^2/g), panels consistently showed higher surface areas, attributed to the compaction process, which enhanced interfacial porosity and exposes additional internal surfaces among granules. Increasing the specific surface area in porous materials enhances acoustic absorption by promoting greater interaction between sound waves and internal surfaces, leading to more effective energy dissipation [61].

Pore size distribution curves (Fig. 7a-b) reveal a shift toward larger pores with increasing H_2O_2 concentration in the granules and acoustic panels. While nanometer-scale pore volume initially decreased at lower concentrations (AP-1 to AP-3) due to rapid bubble formation, higher concentrations (AP-4 and AP-5) demonstrated a distinct increase in pore volume beyond ∼ 50 nm. This increase was less evident in the corresponding granules (G-4 and G-5), highlighting the crucial role of consolidation and compaction during panel fabrication. This process developed interfacial porosity between granules and enhanced nanometer-scale pore connectivity within the structure. Such a structural transformation likely facilitates the formation of a more continuous porous network, which is beneficial for both acoustic performance and mass transport properties [62,63]. The presence of larger voids, ranging from micrometers to millimeters, was confirmed by optical microscopy (Fig. 8) and SEM images (Fig. 11), beyond the detection capabilities of nitrogen adsorption methods [64]. Following the successful consolidation of loose granules into a stable structure, subsequent analysis was conducted to evaluate the acoustic characteristics of the acoustic panels.

The optical microscopy images (Fig. 8) reveal how the pore structure evolved across the X-Y sections of the panels. In AP-R (Fig. 8a), the structure was dominated by large intergranular voids with only limited pores inside the granules, likely due to shrinkage and absence of a foaming agent. With increasing H_2O_2 concentration (1–3 wt%) from AP-1 to AP-3 (Fig. 8b-d), a gradual increase in intragranular pore size and number was observed, while intergranular voids decreased, indicating partial granule expansion and internal pore network growth. At higher concentrations (4–5 wt%) of H_2O_2 (AP-4 and AP-5, Fig. 8e-f), a clear morphological shift occurred. The boundaries between granules became less distinct where pores merged into a more continuous and finely distributed network. This suggests that higher H_2O_2 levels led to better gas dispersion and more uniformity throughout the matrix.

The combined analysis of pore size frequency (Fig. 9) and cumulative pore area (Fig. 10) illustrates how pore structure evolves in alkali-activated geopolymer panels with increasing H_2O_2 content. In this study, dual porosity refers to the coexistence of intergranular voids between granules and intragranular pores within granules which are clearly visible in the optical images (Fig. 8). While intragranular and intergranular porosity contributions are identified and partially quantified (in section 3.2.1), the dual porosity is discussed in terms of observed pore morphology. As pores of comparable sizes occur in both within and among granules, the pore size frequency quantified in Figs. 9 and 10 represents an integrated contribution from intragranular voids and intergranular pores, providing a comprehensive view of the overall porosity distribution. This broad range of pore sizes confirms the hierarchical nature of the structure and supports the presence of dual-level porosity in the panels. The reference sample (AP-R), prepared with DI water exhibited a relatively wide pore size distribution (Fig. 9) centered

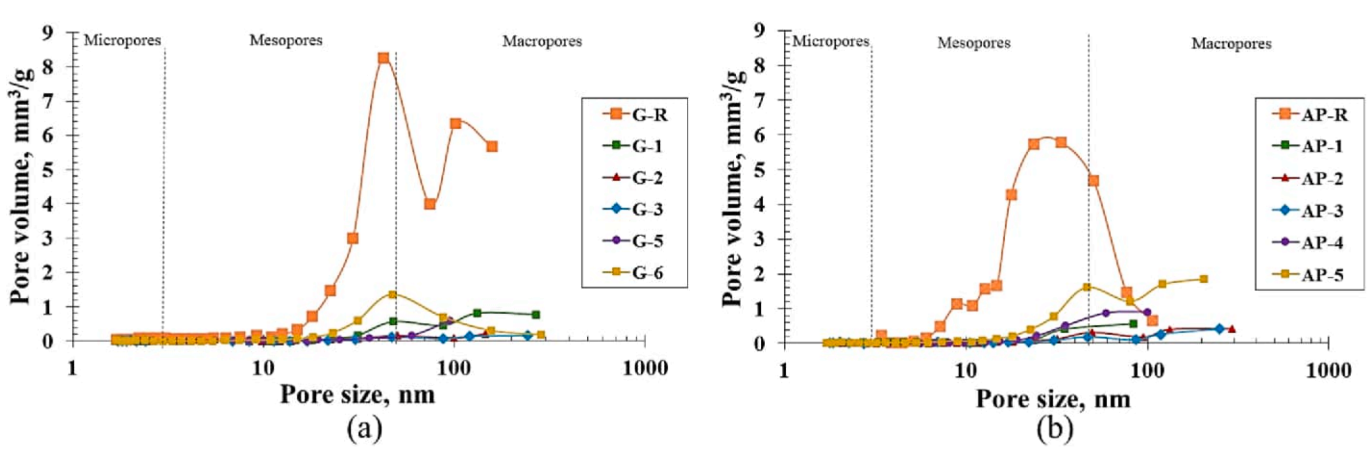

Fig. 7. Pore size distribution curves and cumulative pore volume curves of (a) the loose granules and (b) the acoustic panels.

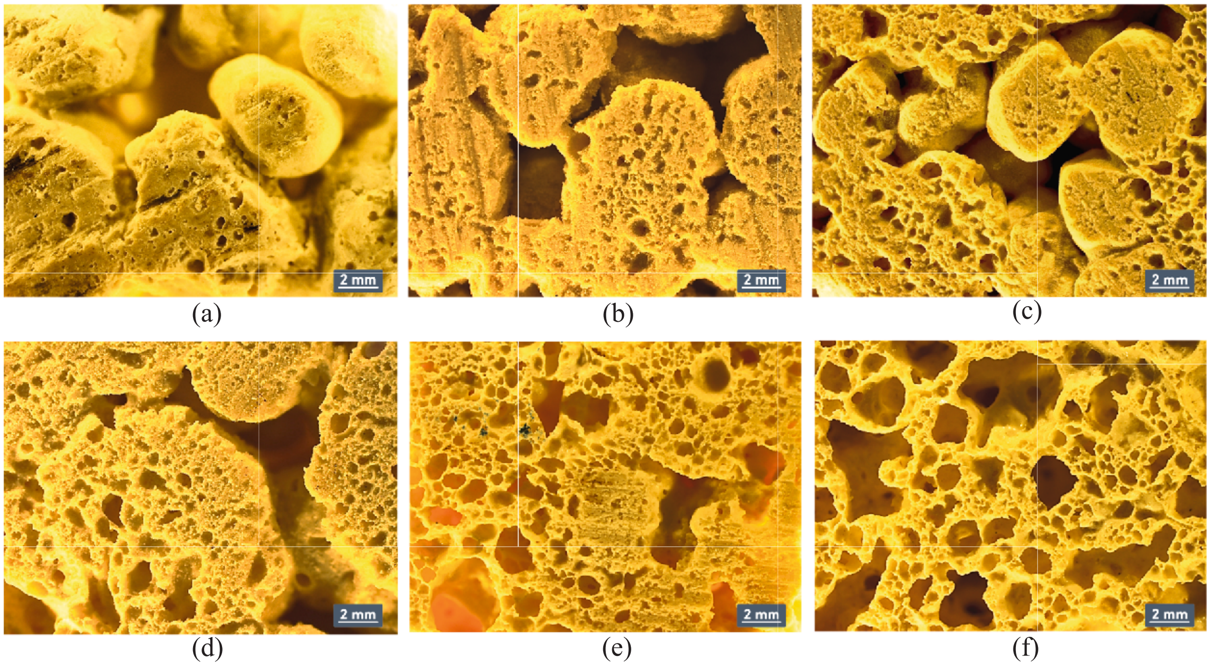

Fig. 8. Acoustic panel imaged from the X-Y cross-sections with optical microscopy (a) AP-R; (b) AP-1; (c) AP-2; (d) AP-3; (e) AP-4 and (f) AP-5.

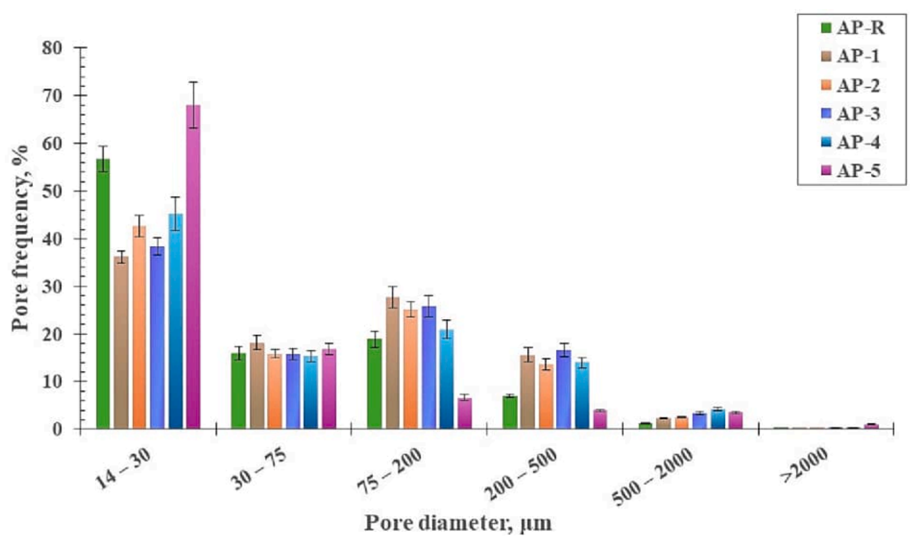

Fig. 9. Frequency distribution of pores categorized by diameter range. The number of pores was grouped into manually defined diameter bins ranging from 14 to > 2000 μm to visualize the distribution of pores sizes in the sample, using consistent bin ranges across all samples for comparative analysis.

around small to medium pores (14–200 μm), with limited cumulative pore area (Fig. 10), reaching just over 30% at larger diameters (~10 μm^2). This indicates minimal gas evolution and mostly intergranular voids caused by drying shrinkage. With 1–4 wt% H_2O_2 (AP-1 to AP-4), the dominant pore size progressively shifted from 14-30 μm to a wider range of 30–500 μm (Fig. 9) exhibiting progressively refined pore structures. Simultaneously, the cumulative pore area (Fig. 10) increased distinctly from AP-2 to AP-4 (reaching up to 55% for AP-4), reflecting improved pore distribution. This was due to improved gas trapping and better setting of the material at medium H_2O_2 concentration levels. Interestingly, AP-5 (5 wt% H_2O_2) departed from this prior trend. Although its cumulative pore area reached 59% (Fig. 10), the dominant pore frequency reverted to 14–30 μm (Fig. 9), which sharply increased to 68%. This suggests dense intragranular pore formation with fewer intergranular voids. The higher H_2O_2 concentration in this study likely caused rapid gas generation, promoting pore growth within the granules while reducing larger intergranular voids. This behavior consistent with Shi et al. [65], who reported that H_2O_2 concentrations up to 3 wt% induced early gas evolution before complete hardening, leading to dense intragranular porosity and fewer intergranular voids in fly ash-metakaolin geopolymer concretes.

To evaluate vertical pore connectivity, SEM analysis of X-Z cross-sections (Fig. 11) was performed aligned with the direction of sound propagation. AP-R displayed a dense structure with isolated pores, while AP-1 to AP-3 showed growing vertical porosity through intragranular expansion and partial merging. AP-4 revealed a homogeneous, continuous pore network with aligned channels, while AP-5 exhibited extensive intragranular porosity with very thin walls as merges with optical microscopy image analyses.

These insights from the analysis of optical microscopy and SEM

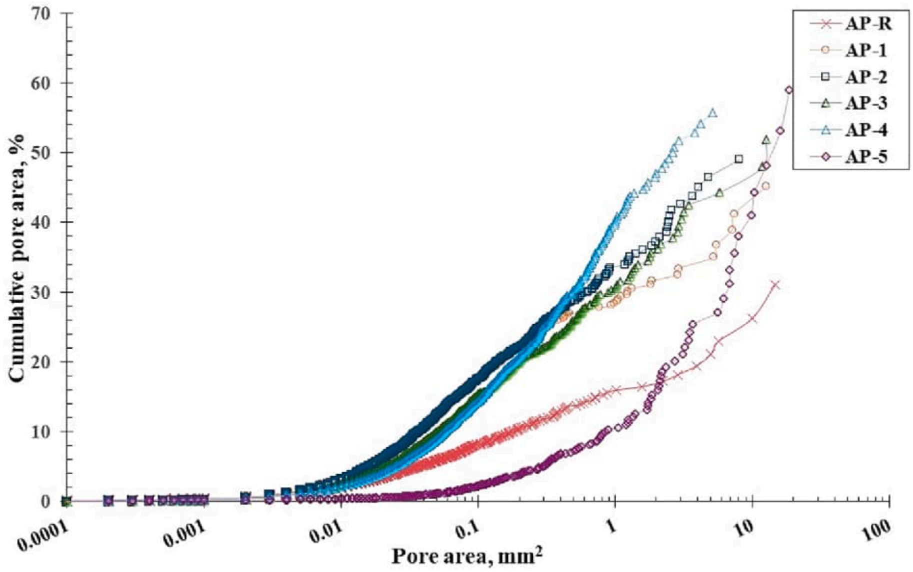

Fig. 10. Cumulative pore area (%) as a function of pore size distribution obtained from 2D optical microscopy analysis of porous acoustic panels. The final value of each curve represents the total porosity of the corresponding panel, indicating the overall percentage of surface area occupied by pores.

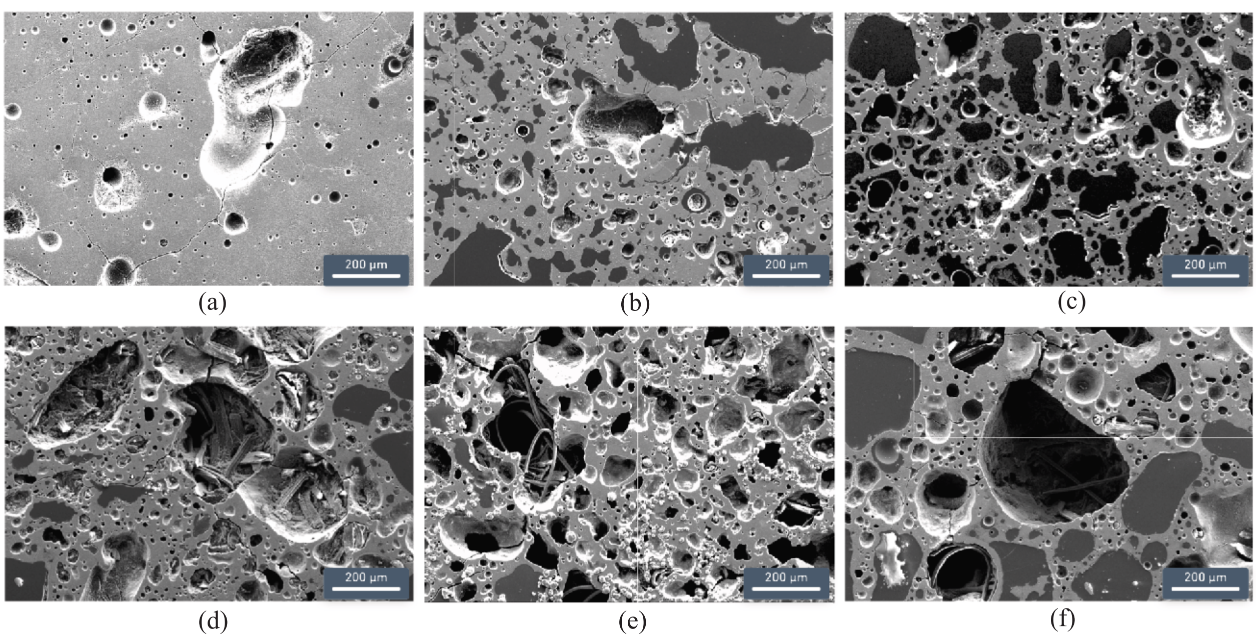

Fig. 11. X-Z cross-sections with scanning electron microscopy (a) AP-R; (b) AP-1; (c) AP-2; (d) AP-3; (e) AP-4 and (f) AP-5.

images demonstrate that increasing concentration of H_2O_2 solution systematically transformed the panel morphology from scattered voids in AP-R to a highly interconnected porous network in AP-4 and AP-5. Such porosity is ideal for sound absorption due to increased internal surface area and pore connectivity [63]. Park et al. [66] showed that sound absorption between 100 and 5000 Hz is typically associated with pore sizes of 1 to 5 mm. The panels developed in this study achieved a broad pore size distribution ranging from nanometers up to approximately 7 mm, supporting effective broadband absorption, as previous research indicates that granular media with such a wide pore size range (nm to mm) significantly enhances sound absorption, particularly at low frequencies relevant to indoor noise (< 500 Hz) [43,67].

3.2.1. Porosity analysis

Archimedes-based porosity represents the total volumetric porosity of the panels, whereas porosity derived from optical microscopy and X-ray microtomography is section-resolved and limited by the spatial resolution of each technique. Consequently, image-based porosity values are particularly used to represent pore morphological evolution.

Porosity values calculated from X-Y cross sections showed a consistent increase with higher H_2O_2 content (Table 4). Porosity

Table 4
Porosity analysis across the horizontal (X-Y) and the vertical (X-Z) cross-section determined from optical microscopy and XCT images, respectively.

Batch ID	X-Y cross section	X-Z cross section
AP-1	45%	28%
AP-3	52%	34%
AP-5	59%	35%

measurements from X-ray microtomography (XCT) of the X-Z sections followed the same trend, though absolute values differed. Optical microscopy employed thinner slices, enabling high-resolution and 2D quantification of fine-scale porosity. In contrast, XCT's lower resolution limited detection of pores smaller than ~ 50 μm due to voxel size constraints required for full sample scanning. Notably, Fig. 9 shows that the dominant pore size contributing to porosity lies between 14–30 μm which is below XCT's detection threshold. Nevertheless, XCT analysis was strategically employed to capture macroscopic structural characteristics, such as pore interconnectivity and granule spatial distribution across the X-Z cross section. These structural characteristics directly influence acoustic attenuation via multiple scattering and dissipation mechanisms [40].

The representative XCT images (Fig. 12a-c) illustrate the progressive development of internal pore structures with increasing H_2O_2 content. Gas evolution produced a tortuous, multi-scale pore network, where larger pores were interconnected by smaller ones [68]. In AP-1 (Fig. 12a), the structure comprised densely packed granules with minimal interconnectivity and distinct intergranular voids, indicating limited structural continuity. In contrast, AP-3 and AP-5 (Fig. 12b-c) showed more open, interconnected frameworks where granule expansion led to particle merging and the formation of an integrated porous network. In AP-5, the upper region exhibited a more pronounced macroporous structure than the lower region, likely due to pore coalescence during foaming. This vertical porosity gradient created a channel network that likely allows sound waves to enter while limiting their escape as suggested by [37]. Notably, in AP-1, dual porosity could be clearly differentiated into two primary categories: intragranular porosity, accounting for 7% of the grain volume, and intergranular porosity, representing 23% of the total sample volume. This dual porosity can enhance both the structural and functional properties of materials, particularly in sound absorption [43]. Cox and D'Antonio [69] also highlighted that combining large pores for sound entry with smaller pores for energy dissipation is essential for effective absorption. This supports the dual-scale pore structure used in this study to enhance broadband acoustic performance.

3.3. Mechanical characterization

Mechanical properties were evaluated to observe the structural integrity and behaviour of the developed panels. The tests were conducted under quasi-static loading to represent strength and stiffness associated with the processing-induced pore structure. The panels developed in this study achieved flexural strengths between 0.60 and 1.20 MPa under maximum load (Fig. 13a). In reference to prior work, Bartolini et al. [25] reported a flexural strength of 0.62 MPa for a resin-bonded granular acoustic absorber, indicating that the current panels achieved comparable or higher strength without additional binders despite having a similar density profile. The AP-1 panel (1 wt% H_2O_2) showed a threefold increase in strength compared to the reference sample AP-R (DI water). However, higher H_2O_2 concentrations did not lead to further improvement. Instead, the strength values for AP-1 to AP-4 remained relatively stable with slight fluctuations. A significant reduction was observed in AP-5, which had approximately half the strength of the other H_2O_2-treated samples. The overall trend was AP-1 ≈ AP-2 > AP-4 ≈ AP-3 > AP-5 > AP-R. The elastic modulus followed a similar pattern. AP-R exhibited the lowest modulus at 49 ± 7 MPa, while AP-1 achieved the highest at 137 ± 35 MPa. Modulus values for AP-2 to AP-4 varied between 66 ± 7 and 95 ± 8 MPa, and AP-5 dropped again to 53 ± 13 MPa.

The granular panel developed in this study exhibited compressive strengths up to three times higher than those reported by Bartolini et al. [25] for an epoxy-bonded granular acoustic absorber (1.25) of similar density. The compressive strength (Fig. 13b) of acoustic panels containing H_2O_2 generally surpassed that of the reference sample (AP-R), with AP-1, AP-2, and AP-3 exhibiting up to four times greater strength. The strength trend followed: AP-2 > AP-3 > AP-1 > AP-4 > AP-5 > AP-R, showing a similar pattern to the flexural strength but with clearer differentiation. The elastic modulus values from the compression test followed a similar trend to the flexural strength results. AP-R exhibited the lowest modulus at 27 ± 12 MPa, while AP-1 showed the highest modulus at 1575 ± 248 MPa. The modulus values for AP-2 to AP-4 ranged between 1310 ± 130 MPa and 806 ± 90 MPa, reflecting a gradual decrease as the H_2O_2 concentration increased. Finally, AP-5 exhibited a notable drop in modulus, with a value of 362 ± 47 MPa, suggesting that higher H_2O_2 concentrations reduce the material's stiffness. Both compressive and flexural tests revealed a notable increase in strength with the inclusion of 1–2 wt% H_2O_2 solution, whereas concentrations of 3–5 wt% solutions led to a gradual reduction in strength. These findings suggest that low concentrations of H_2O_2 solutions (1–2 wt%) are associated with higher stiffness and strength of the panels as the foaming effect from 1 to 2% H_2O_2 improved interconnectivity in AP-1 and AP-2, resulting in stronger panels compared to the more brittle AP-R. Conversely, higher levels may compromise mechanical integrity, aligning with observed structural changes as the higher porosity of AP-3 to AP-5 (with 3–5 wt% H_2O_2 solutions) (detailed in Section 3.2) led to lower density and reduced strength despite improved interconnectivity. Elastic modulus values are reported here as mean ± standard deviation

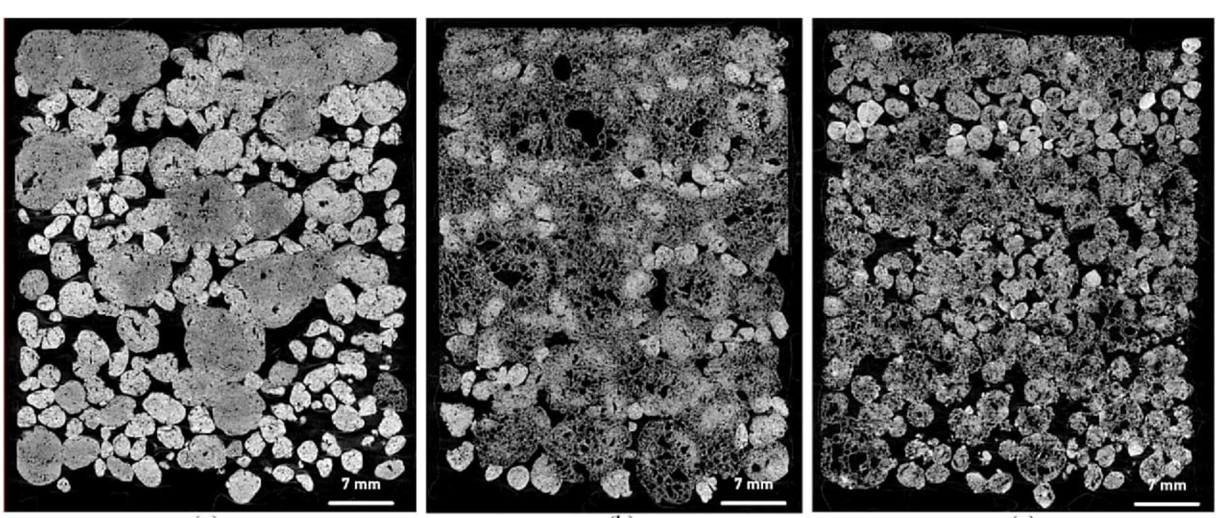

Fig. 12. X-Z cross section imaging by X-ray microtomography: (a) AP-1; (b) AP-3 and (c) Ap-5.

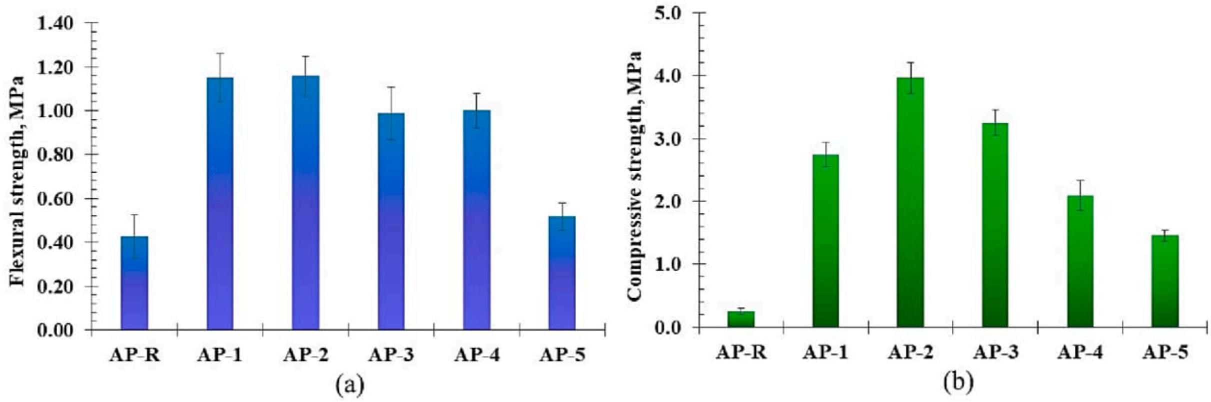

Fig. 13. Strength evaluation of induvial acoustic panel. (a) Flexural strength and (b) Compressive strength of. 6 samples were measured for each bar.

based on six specimens per panel. One-way ANOVA indicated statistically significant differences in elastic modulus among the panel groups ($p < 0.05$).

Fig. 14 presents the load–displacement behavior of an AP-1 panel as a representative case, demonstrating the results from both the three-point flexural test (Fig. 14a) and the compression test (Fig. 14b). The fracture occurred progressively rather than as a single sudden event, as seen from the multiple peaks in the load–displacement curves. This gradual failure is influenced by the heterogeneous and multi-scale pore structure inherent to the granular system, where crack propagation and the sequential fracture of individual granules (Fig. 14c) contributed to the overall response. For consistency, the failure point was defined as the first peak load prior to the major drop in the curve. This behavior reflects the influence of structural heterogeneity on crack initiation and propagation within the granular network.

3.4. Acoustical properties

3.4.1. Acoustical tests

Fig. 15 represents the normal incidence sound absorption coefficient of individual acoustic panels. Overall, all the samples prepared with DI water (AP-R) and 1–5 wt% H_2O_2 solutions (AP-1 to AP-5) absorbed more than 30% to maximum 93% of sound over the frequency range from 200 to 4300 Hz. The absorption profile for the AP-R sample (Fig. 15a) exhibited two distinct sharp peaks: a primary peak near 1000 Hz and a secondary one around 3300 Hz where the absorption coefficient α was found to be ≈ 0.95 and ≈ 0.88, respectively. Besides that, the absorption was not found to be effective throughout frequencies, especially between 1500–3000 Hz, the absorption is significantly lower (α < 0.4). AP-R had almost similar open porosity as the other H_2O_2 treated samples. In the absence of a foaming agent, the granules underwent shrinkage rather than expansion, which heavily leads to the creation of inter granular space, however porosity within the granules was not found much as described in section 3.2. Likely due to low porosity and fewer tortuous air pathways, sound energy was only efficiently dissipated at specific resonant frequencies. This suggests that AP-R behaved like a resonator-based material, with well-defined peaks where the material geometry and internal structure (possibly from granule packing and binder bridges) matched sound wave patterns at specific frequencies [70], where sound energy was efficiently converted into heat. This behavior can be attributed to tightly packed granules forming enclosed and partially connected air cavities that trap sound waves and enhance viscous and thermal energy dissipation within the porous framework. Moreover, the sound absorption of granular materials is related to flow resistance, porosity and structure factor, and finally attributed to the pellets gap. When the gap is too large or too small, insufficient friction and heat exchange occur during the propagation of sound waves, which results in reduced sound absorption efficiency [71].

AP-1 (Fig. 15b), prepared with 1 wt% H_2O_2 solution, exhibited a hybrid absorption profile, combining a sharp resonance peak near 500 Hz and a broader peak around 3500 Hz extending into a plateau beyond 4000 Hz. This suggests that even a minimal amount of H_2O_2 induced the formation of interconnected pores, enhancing tortuosity and thus sound energy dissipation. AP-1 thus transitioned from pure resonant absorption (as in AP-R) toward a mixed-mode mechanism that combined cavity resonance with porous damping for tunable broadband performance [72]. AP-2 (Fig. 15c), in contrast, showed a broader and more distributed absorption response between 500–4000 Hz which suggests a shift toward classical porous absorber behavior, likely due to a more aerated microstructures, enhancing flow resistivity and internal friction which are the key factors in dissipating acoustic energy across a wider frequency range [73]. The absorption coefficient α showed approximately

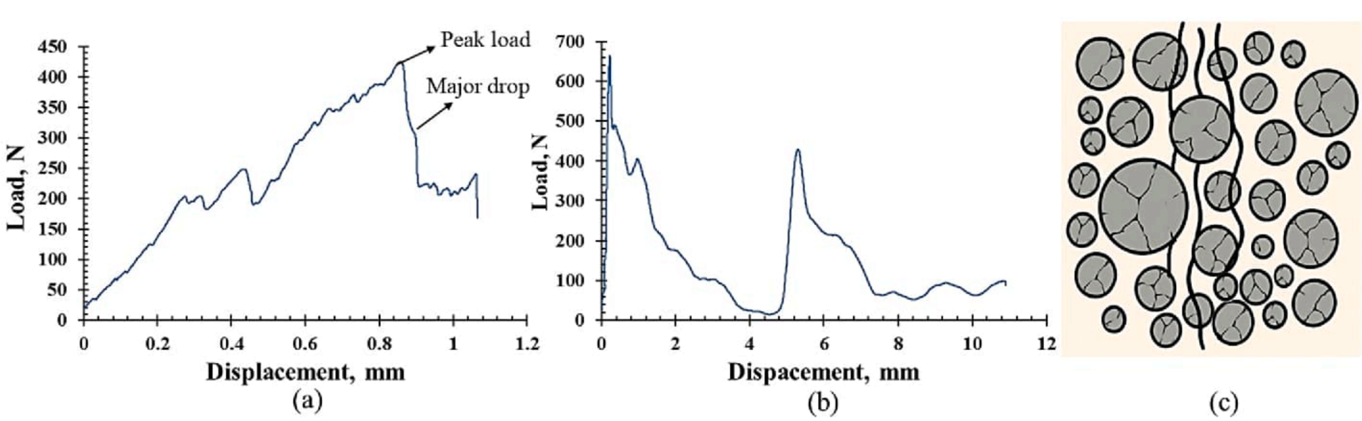

Fig. 14. Load-displacement curve from (a) flexure test; (b) compression test and (c) conceptual view of progressive crack propagation.

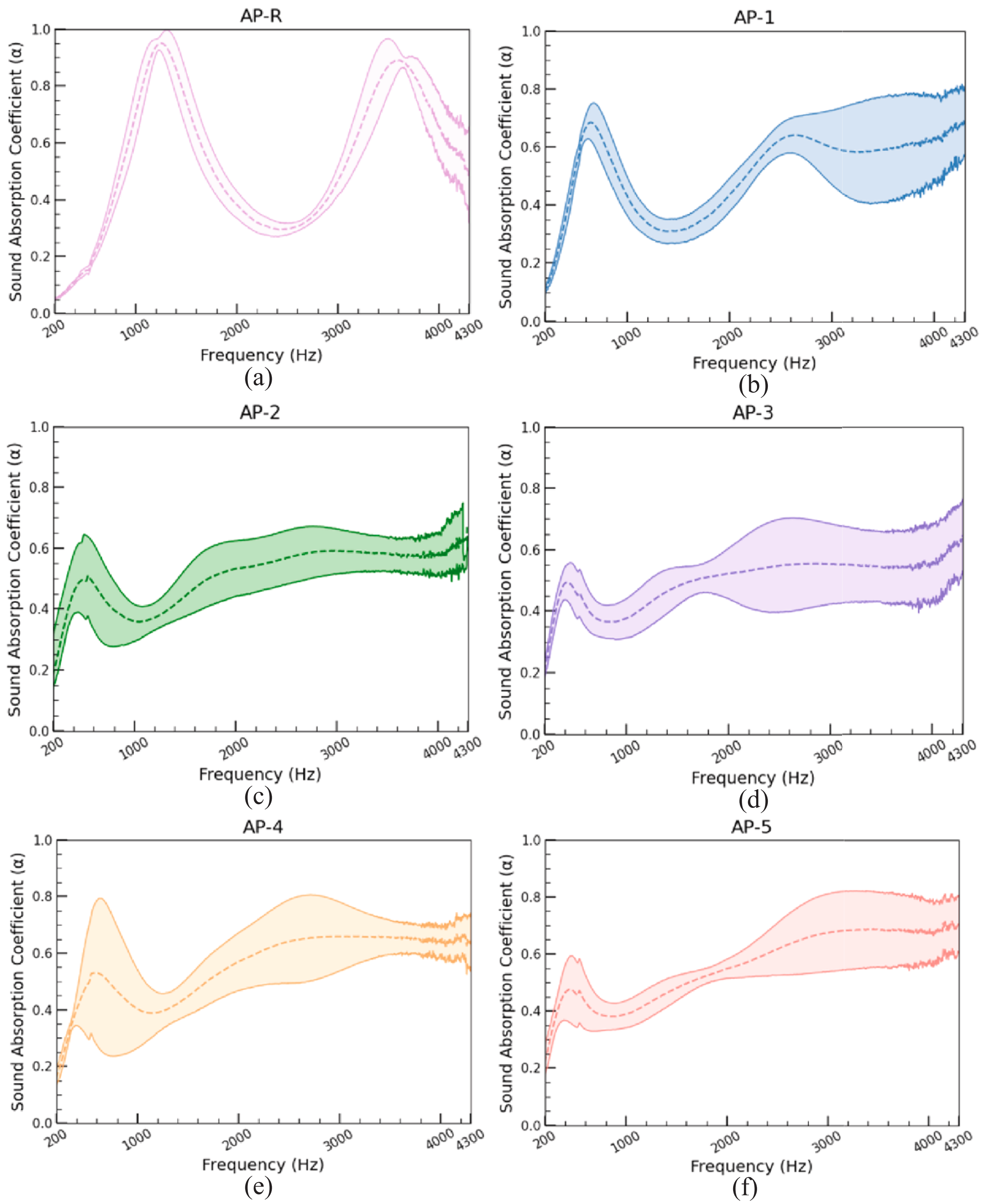

Fig. 15. Each plot shows the normal incidence sound absorption coefficient (α) over a frequency range of 200–4300 Hz (6 specimens per batch). The dotted line represents the average value of α. The shaded region indicates the maximum and minimum value at each frequency.

0.47 near 950 Hz, followed by a gradual rise to ≈ 0.70 at 4000 Hz. These results indicated that, compared to AP-1, pore development has progressed, improving performance particularly in the mid to high-frequency range (above 1500 Hz).

AP-3 (Fig. 15d) showed smoother absorption across the frequency spectrum with a moderate low-frequency absorption α ≈ 0.45 at 700 Hz and a rise to ≈ 0.75 above 4000 Hz. This behavior suggests a more advanced pore network, likely formed through increased H_2O_2 content contributing to an increase in absorption performance, especially at higher frequencies. However, the less intense peaks may indicate the presence of over-aerated or coalesced pores, which could reduce tortuosity or disrupt the optimal pore structure leading to impedance mismatches, diminishing absorption efficiency at low frequencies [40]. AP-4 (Fig. 15e) presented dual higher absorption behavior (≈ 0.55 at 1000 Hz and ≈ 0.78 at 3800–4000 Hz), similar to AP-1, but with overall better absorption performance. These results suggest that higher hydrogen peroxide (H_2O_2) content enhanced the material's resonance and scattering capabilities at lower frequencies. This comparatively higher broadband absorption can be attributed to increased tortuosity and pore connectivity, which contributed to more effective sound absorption across a wider frequency range.

AP-5 (Fig. 15f) delivered the highest absorption performance at high frequencies among the modified samples (≈ 0.42 at 800 Hz rising to ≈ 0.80 at 4000 Hz) as well as effective sound absorption across a broad spectrum. The highly porous and interconnected structure supported both thermal and viscous energy dissipation, making it suitable for applications in interior building elements where high-frequency sound control is critical, such as in reducing reverberation and improving room acoustics [74]. Studies on the acoustic performance of building materials highlight the significance of high-frequency absorption for controlling sound reflection and enhancing indoor acoustics [72]. The developed pore structure likely influenced airflow resistivity while having sufficient open porosity for sound wave penetration, thereby enhancing viscous and thermal energy dissipation and maximizing performance [71,72]. In general, increasing H_2O_2 concentration progressively increased pore connectivity, tortuosity, and open porosity which likely altered the acoustic impedance of the material, leading the progressive broadening of observed dominant absorption features but within the similar frequency regions and indicating that the absorption behavior is governed by changes in airflow resistivity and pore structure rather than the formation of new resonant modes. This evolution reflects a transition from localized resonance-dominated behavior to broadband porous absorption influenced by viscous-thermal losses in the air phase [40,70,72]. This structural evolution enables improved acoustic performance across wider frequency ranges, particularly in the mid to high frequency spectrum.

3.4.2. *Correlation of tortuosity with acoustic absorption behavior*

The evolution in sound absorption behavior observed across samples AP-1, AP-3, and AP-5 shows a consistent trend with changes in measured tortuosity (Table 5), which increased with higher H_2O_2 content. Tortuosity is associated with high-frequency sound absorption within the samples investigated, as it represents the complexity of internal pathways through which sound must propagate. In AP-1, the relatively low tortuosity correlates with the material's hybrid profile retaining a sharp resonant peak at low frequencies (≈ 500 Hz) while starting broader porous absorption beyond 3500 Hz. As tortuosity increases in AP-3, the absorption curve becomes smoother, and broadband performance improves, suggesting enhanced pore interconnectivity. However, moderate tortuosity may indicate that some over-aeration or pore coalescence may reduce structural complexity, impacting peak intensity as mentioned in section 3.4. In contrast, AP-5, with the highest tortuosity, a comparatively higher broadband response among the samples studied, particularly above 2000 Hz. The increased tortuosity in this case is associated with longer and more intricate flow paths, which may enhance viscous and thermal dissipation and contribute to increased acoustic attenuation at higher frequencies within the studied range. These findings align with the theoretical framework presented by Allard & Atalla [40], which emphasizes tortuosity as a key parameter in enhancing high-frequency acoustic performance in porous materials. Typical tortuosity values for granular absorbers range between 1.10 and 1.80, [69] and the panels developed in this study fall well within this range, indicating transport characteristics consistent with granular porous absorbers.

Table 5
Tortuosity of the acoustic panels.

Batch ID	Tortuosity
AP-1	1.20
AP-3	1.32
AP-5	1.60

4. Discussion

As noted by Allard & Atalla [40], acoustic materials which contain open porosity below 20% (fraction of open pores within the total porosity) tend to absorb better at low frequencies but poorly at higher frequencies. Developed panels in this study demonstrated open porosity higher than 20% (Fig. 6), so the relatively weaker low-frequency absorption and stronger mid-to-high frequency performance are expected. This suggests that pore structure plays a major role in influencing acoustic behavior of the panels. The broad and consistent absorption observed across AP-1 to AP-5 supports this, aligning with design principles for multilayer porous materials [69,75]. Empirical analysis revealed a consistent relationship between the pore structure and the acoustic response of the panels. With increasing H_2O_2 concentration, open porosity increased from 24.8% to 39%, while tortuosity rose from 1.2 to 1.6, reflecting enhanced intergranular connectivity. These microstructural modifications were accompanied by a downward shift of the main absorption peak from approximately 1000 Hz to 500 Hz and a broadening of the absorption bandwidth. The results indicate that larger and more interconnected pores are associated with improved air movement and viscous dissipation, contributing to enhanced low-frequency attenuation, whereas finer intragranular pores are associated with increased high-frequency absorption. The acoustic response is therefore interpreted as the result of the combined influence of pore morphology and tortuosity, which evolve simultaneously with the processing conditions.

As summarized in Table 6, panels containing a higher proportion of small pores (15–30 μm), such as AP-R and AP-5, exhibited improved mid- to high-frequency absorption, while AP-R showed negligible absorption at low frequencies, confirming that smaller pores are less effective for long-wavelength attenuation. This observation is consistent with the findings of Liu and Nagel [56], who reported that at high frequencies, when the sound wavelength (λ) becomes comparable to the pore or grain size, scattering and local resonances dominate the energy dissipation. Between AP-1 and AP-2, the appearance of medium pores (75–500 μm) led to an increase in low-frequency absorption, whereas AP-3 and AP-4, characterized by a balanced distribution of small, medium, and large pores, achieved the most uniform broadband performance. Notably, AP-5 maintained comparable low-frequency absorption despite containing fewer 75–200 μm pores, likely due to its higher pore interconnectivity and the presence of very large pores (> 500 μm, ≈ 6%) (as discussed in Section 3.2). Such a structure likely enabled better low-frequency sound attenuation, as larger pores help absorb longer sound wavelengths (λ), supporting the relationship identified by Liu and Nagel [56]. Additionally, the continuous interconnected structure of AP-5 allowed the entire panel to damp vibrations effectively, which is particularly relevant since low-frequency sounds can also manifest as vibrations. Therefore, its ability to attenuate low-frequency sound despite having fewer large pores may result not only from pore-scale absorption but also from bulk vibration damping. Overall, these empirical findings highlight that panels produced with moderate foaming levels (3–5 wt% H_2O_2 solutions) develop a hierarchical pore structure that supports broadband sound absorption through the coupled effects of pore size, connectivity, and tortuosity.

The mechanical behavior of the lightweight geopolymer panels reflects the characteristic balance between porosity and structural strength observed in alkali-activated porous systems. Increasing pore content and interconnectivity reduced density and increased brittleness, as commonly reported for geopolymer foams [76]. Reported compressive strengths for comparable lightweight materials range from 0.75-3.6 MPa [76,77], with flexural strengths between 1.1–3.7 MPa [78,79], consistent with the values obtained for panels AP-2 to AP-4 in this study. The interconnected pore network and strong intergranular bonding contributed not only to adequate mechanical rigidity but also to increase acoustic efficiency, since the same structural continuity supports viscous and thermal energy dissipation across multiple scales. This

Table 6
Pore size frequency (%) of the panels and their corresponding average sound absorption performance; minor pore fractions (including 500–2000 μm and > 2000 μm) are not included. The complete pore size distribution is provided in Fig. 9.

Batch ID	Percentage distribution of dominant pore size ranges				Average normal incidence sound absorption coefficient, α		
	15–30 μm	30–75 μm	75–200 μm	200–500 μm	Low frequency (< 500 Hz)	Mid frequency (500–2000 Hz)	High frequency (2000–4000 Hz)
AP-R	56%	16%	20%	6%	0.09	0.50	0.60
AP-1	36%	18%	26%	16%	0.35	0.44	0.53
AP-2	42%	16%	25%	15%	0.31	0.40	0.58
AP-3	38%	16%	26%	16%	0.37	0.48	0.55
AP-4	46%	16%	22%	15%	0.31	0.46	0.60
AP-5	68%	18%	6%	4%	0.37	0.45	0.65
Commercial polyurethane foam					0.15	0.40	0.70
Melamine foams					0.20	0.30	0.56

microstructure-driven synergy distinguishes the panels from conventional polymeric absorbers such as polyurethane (PU) [16] and melamine foams (MF) [80]. Although the overall sound absorption performance is comparable at mid to high frequencies (Table 6), the geopolymer panels (50 mm thick) achieve superior low-frequency absorption and exhibit compressive strengths in the MPa range, compared to 13–38 kPa for 40 mm thick PU foam [81] and ~ 14 kPa for 20 mm thick MF foam [80]. The substantially higher compressive strength provides the mechanical integrity necessary for structural rigidity and shape retention while effectively dissipating sound energy to enhance absorption performance [82]. Based on the measured mechanical strength, the panels may have potential applicability in building acoustic elements such as wall linings and ceiling panels, as well as in resilient layers used in floating floor systems [83–85].

Table 7 presents a thickness-matched comparison of the octave-band absorption of AP-4 and AP-5 with a 50 mm polyurethane foam. The developed panels show absorption levels comparable to polyurethane foam over the mid- and high-frequency ranges, with similar performance observed around 500–4000 Hz. This comparison provides an indicative benchmark at equal thickness, noting that the acoustic performance of commercial materials may vary with product characteristics and mounting conditions. Together, these findings confirm that the developed geopolymer panels combine broadband acoustic absorption, mechanical robustness, and inherent fire and thermal resistance, demonstrating clear potential as viable alternatives to conventional absorbers, with the added advantage of reducing the need for supplementary protective layers [86].

5. Conclusions

This study aimed to address the demand for sustainable, binder-free acoustic materials by developing H_2O_2-treated granular composite panels with influenced pore structures. By systematically varying the H_2O_2 content, it was possible to achieve adequate porosity and tortuosity while maintaining acceptable mechanical stability. All panels produced with 1–5% H_2O_2 solution granulation doses consistently exhibited high porosity (60–70%) and effective sound absorption across a wide frequency range (250–4300 Hz), highlighting their suitability for broadband acoustic applications. Among them, the panels prepared with 4 wt% and 5 wt% H_2O_2 solutions exhibited the highest overall acoustic performance. The panel prepared with 4 wt% H_2O_2 solution achieved an absorption coefficient increasing from ≈ 0.55 at 1000 Hz to ≈ 0.78 at 3800–4000 Hz, while the 5 wt% H_2O_2 panel increased from ≈ 0.42 at 800 Hz to ≈ 0.80 at 4000 Hz. Notably, the 4 wt% H_2O_2 panel performed better at frequencies below 1000 Hz. This improvement for both panels was attributed to a highly interconnected and tortuous pore network, which facilitated enhanced viscous and thermal dissipation mechanisms, particularly at mid to high frequencies (500–4300 Hz).

Table 7
Octave-band normal-incidence sound absorption coefficients of the developed panels (AP-4 and AP-5) compared with a 50 mm polyurethane foam [87] (thickness-matched comparison).

Material	250 Hz	500 Hz	1000 Hz	2000 Hz	4000 Hz
Polyutherane foam (50 mm)	0.40	0.65	0.55	0.70	0.70
AP-4	0.30	0.55	0.60	0.60	0.70
AP-5	0.40	0.55	0.40	0.60	0.70

The self-consolidating process yielded stable microstructural and acoustic properties without external binders, confirming viability for applications where integrity and reproducibility are critical. Limitations remain in the low-frequency range, and the roles of particle size distribution and closed porosity require further study. Future investigations should consider hybrid foaming or multilayer configurations to enhance low-frequency performance as well as the use of recycled/bio-based fillers to reduce environmental impact, and computational modeling to guide optimization. Moreover, the reported acoustic performance is based on normal-incidence measurements (ISO 10534–2); therefore, the results represent material-level behavior, and performance under diffuse field conditions may differ and require further evaluation using reverberation room measurements.

In summary, the most influential factors for improving acoustic performance in porous geopolymers are: (i) pore connectivity that establishes continuous air pathways, (ii) tortuosity that increases effective path length and viscous/thermal losses, and (iii) a balanced pore-size hierarchy (dual porosity) combining finer intragranular pores with larger intergranular pores. Within this framework, moderate H_2O_2 solutions dosing (3–5 wt%) provides a practical route to module these parameters simultaneously. Considering the demonstrated MPa-level compressive strength, the panels are competitive with conventional absorbers at comparable thickness, particularly due to better low-frequency absorption. These findings suggest that, with appropriate modifications and standardization, the panels have potential for use as indoor building materials for sound absorption.

6. Data Availability

The data supporting the findings of this study are openly available at doi:10.23729/fd-7e85cf6e-0079-3e85-80f6-c4203690d890.

CRediT authorship contribution statement

Nusrat Kabir: Writing – original draft, Visualization, Validation, Methodology, Investigation, Formal analysis, Conceptualization. **Tero Luukkonen:** Writing – review & editing, Supervision, Methodology, Conceptualization. **Johan Augusto Bocanegra:** Writing – review & editing, Validation, Resources, Investigation. **Davide Borelli:** Writing – review & editing, Validation, Resources, Investigation. **Priyadharshini Perumal:** Writing – review & editing, Supervision, Methodology, Funding acquisition, Conceptualization.

Declaration of competing interest

The authors declare that they have no known competing financial interests or personal relationships that could have appeared to influence the work reported in this paper.

Acknowledgement

Authors like to acknowledge the support provided as part of Horizon Europe EXCEED project (Grant Agreement No. 101091543), AshCycle project (Grant Agreement No. 101058162) funded by the European Union and REMIS project (BFRK/618/31/2024) funded by Business Finland, Finland. X-ray computed tomography was supported by the RAMI infrastructure project (#293109) funded by Research Council of Finland, Finland. Prof. Corrado Schenone is gratefully acknowledged for providing the equipment utilized in this study for acoustic tests.

Appendix A. Supplementary data

Supplementary data to this article can be found online at https://doi.org/10.1016/j.apacoust.2026.111332.

References

[1] Bronzaft AL, Hagler L. Noise: the invisible pollutant that cannot be ignored. In: Shah V, editor. Emerging Environmental Technologies, Volume II. Dordrecht: Springer; 2010. p. 75–96. https://doi.org/10.1007/978-90-481-3352-9_4.
[2] Klatte M, Bergström K, Lachmann T. Does noise affect learning? a short review on noise effects on cognitive performance in children. Front Psychol 2013;4:578. https://doi.org/10.3389/fpsyg.2013.00578.
[3] Astolfi A, Puglisi GE, Murgia S, Minelli G, Pellerey F, Prato A, et al. Influence of classroom acoustics on noise disturbance and well-being for first graders. Front Psychol 2019;10:2736. https://doi.org/10.3389/fpsyg.2019.02736.
[4] Hsu T, Ryherd EE, Waye KP, Ackerman J. Noise pollution in hospitals: impact on patients. J Clin Outcomes Manag 2012;19:301–9. https://www.researchgate.net/publication/255966407_Noise_pollution_in_hospitals_Impact_on_patients.
[5] Singh N, Davar SC. Noise pollution: sources, effects and control. J Hum Ecol 2004;16:181–7. https://doi.org/10.1080/09709274.2004.11905735.
[6] Jariwala HJ, Syed HS, Pandya MJ, Gajera YM. Noise pollution and human health: a review. In: Conference: Noise and Air Pollution: Challenges and Opportunities; 2017. p. 1–4.
[7] Berglund B, Lindvall T, Schwela DH. Guidelines for community noise. Noise Vibr Worldwide 1995;31:1–141. https://doi.org/10.1260/0957456001497535.
[8] Adetoun Mustapha BA, Blangiardo M, Briggs DJ, Hansell AL. Traffic air pollution and other risk factors for respiratory illness in schoolchildren in the Niger-delta region of Nigeria. Environ Health Perspect 2011;119:1478–82. https://doi.org/10.1289/ehp.1003099.
[9] Fang X, Pan X, Zhang X, Li D, Yin X, Jin Y, et al. Investigation on low-frequency and broadband sound absorption of the compact anechoic coating considering hydrostatic pressure. Journal of Marine Science and Engineering 2024;12:543. https://doi.org/10.3390/jmse12040543.
[10] Maderuelo-Sanz R, Nadal-Gisbert AV, Crespo-Amorós JE, Morillas JMB, Parres-García F, Sanchis EJ. Influence of the microstructure on the acoustical performance of consolidated lightweight granular materials. Acoust Aust 2016;44:357–64. https://doi.org/10.1007/s40857-016-0048-5.
[11] Hassani P, Soltani P, Ghane M, Zarrebini M. Porous resin-bonded recycled denim composite as an efficient sound-absorbing material. Appl Acoust 2021;173:107710. https://doi.org/10.1016/j.apacoust.2020.107710.
[12] Ramamoorthy M, Rengasamy RS. Study on the effects of denier and shapes of polyester fibres on acoustic performance of needle-punched nonwovens with air-gap: comparison of artificial neural network and regression modelling approaches to predict the sound absorption coefficient of nonwovens. J Text Inst 2019;110:315–27. https://doi.org/10.1080/00405000.2018.1512834.
[13] Soltani P, Azimian M, Wiegmann A, Zarrebini M. Experimental and computational analysis of sound absorption behavior in needled nonwovens. J Sound Vib 2018;426:1–15. https://doi.org/10.1016/j.jsv.2018.04.007.
[14] Aso S, Kinoshita R. Sound absorption coefficient of glass wool. Journal of the Textile Machinery Society of Japan (Transactions) 1965;18:T649–53. https://doi.org/10.4188/transjtmsj1965b.18.t649.
[15] Uris A, Llopis A, Llinares J. Effect of the rockwool bulk density on the airborne sound insulation of lightweight double walls. Appl Acoust 1999;58:327–44. https://doi.org/10.1016/S0003-682X(98)00065-6.
[16] Chanlert P, Jintara A, Manoma W. Comparison of the sound absorption properties of acoustic absorbers made from used copy paper and corrugated board. BioResources 2022;17:5612–21. https://doi.org/10.15376/biores.17.4.5612-5621.
[17] Ehsan Samaei S, Berardi U, Taban E, Soltani P, Mohammad Mousavi S. Natural fibro-granular composite as a novel sustainable sound-absorbing material. Appl Acoust 2021;181:108157. https://doi.org/10.1016/j.apacoust.2021.108157.
[18] G. Pispola K.V. Horoshenkov Consolidated granular media for sound insulation: performance evaluation through different methods 2005 Lisbon, Portugal 260 267.
[19] Kim KW, Lim HM, Yoon SY, Ko H. Fast-curing geopolymer foams with an enhanced pore homogeneity derived by hydrogen peroxide and sodium dodecyl sulfate surfactant. Minerals 2022;12:821. https://doi.org/10.3390/min12070821.
[20] Badri Y, Dodd G, Cater J, Hall A, Schmid G, Emms G, et al. Review of granular material damping and sound absorption for possible application in the sound insulation of lightweight floors. Journal of Building Engineering 2024;97:110881. https://doi.org/10.1016/j.jobe.2024.110881.
[21] Przychodzień P, Katzer J. Properties of structural lightweight aggregate concrete based on sintered fly ash and modified with exfoliated vermiculite. Materials 2021;14:5922. https://doi.org/10.3390/ma14205922.
[22] Tataranni P, Besemer GM, Bortolotti V, Sangiorgi C. Preliminary research on the physical and mechanical properties of alternative lightweight aggregates produced by alkali-activation of waste powders. Materials 2018;11:1255. https://doi.org/10.3390/ma11071255.
[23] Horoshenkov KV, Swift MJ. The acoustic properties of granular materials with pore size distribution close to log-normal. J Acoust Soc Am 2001;110:2371–8. https://doi.org/10.1121/1.1408312.
[24] Pfretzschner J, Rodriguez RM. Acoustic properties of rubber crumbs. Polym Test 1999;18:81–92. https://doi.org/10.1016/S0142-9418(98)00009-9.
[25] Bartolini R, Filippozzi S, Princi E, Schenone C, Vicini S. Acoustic and mechanical properties of expanded clay granulates consolidated by epoxy resin. Appl Clay Sci 2010;48:460–5. https://doi.org/10.1016/j.clay.2010.02.007.
[26] Vašina M, Hughes DC, Horoshenkov KV, Lapčík L. The acoustical properties of consolidated expanded clay granulates. Appl Acoust 2006;67:787–96. https://doi.org/10.1016/j.apacoust.2005.08.003.
[27] Benkreira H, Khan A, Horoshenkov KV. Sustainable acoustic and thermal insulation materials from elastomeric waste residues. Chem Eng Sci 2011;66:4157–71. https://doi.org/10.1016/j.ces.2011.05.047.
[28] El Dandachy ME, Hassoun P, El-Mir A, Khatib JM. Effect of elevated temperatures on compressive strength, ultrasonic pulse velocity, and transfer properties of metakaolin-based geopolymer mortars. Buildings 2024;14:2126. https://doi.org/10.3390/buildings14072126.
[29] Hwang C-Y, Lo Y-M, Abdullah MMAB, Zulkifly K, Ng H-T, Heah Y-J, et al. Elevated temperatures exposure of geopolymers. In: Geopolymers. CRC Press; 2023. https://doi.org/10.1201/9781003390190-7.
[30] Hamdane H, Tamraoui Y, Mansouri S, Oumam M, Bouih A, El Ghailassi T, et al. Statistical modeling of geopolymers from dual-alkali activation of un-calcined phosphate sludge and their potential applications as sustainable coating materials. J Clean Prod 2021;283:125421. https://doi.org/10.1016/j.jclepro.2020.125421.
[31] Komnitsas KA. Potential of geopolymer technology towards green buildings and sustainable cities. Procedia Eng 2011;21:1023–32. https://doi.org/10.1016/j.proeng.2011.11.2108.
[32] Shehata N, Mohamed OA, Sayed ET, Abdelkareem MA, Olabi AG. Geopolymer concrete as green building materials: recent applications, sustainable development and circular economy potentials. Sci Total Environ 2022;836:155577. https://doi.org/10.1016/j.scitotenv.2022.155577.
[33] Xu J, Li M, Zhao D, Zhong G, Sun Y, Hu X, et al. Research and application progress of geopolymers in adsorption: a review. Nanomaterials 2022;12:3002. https://doi.org/10.3390/nano12173002.
[34] Siyal AA, Shamsuddin MR, Khan MI, Rabat NE, Zulfiqar M, Man Z, et al. A review on geopolymers as emerging materials for the adsorption of heavy metals and dyes. J Environ Manage 2018;224:327–39. https://doi.org/10.1016/j.jenvman.2018.07.046.
[35] Neville AM. *Properties of concrete*. 5th ed. Harlow, UK: Pearson Education Limited; 2011.
[36] Yu Y, Perumal P, Corfe IJ, Paul T, Illikainen M, Luukkonen T. Combined granulation–alkali activation–direct foaming process: a novel route to porous geopolymer granules with enhanced adsorption properties. Mater Des 2023;227:111781. https://doi.org/10.1016/j.matdes.2023.111781.
[37] Leiva C, Luna-Galiano Y, Arenas C, Alonso-Fariñas B, Fernández-Pereira C. A porous geopolymer based on aluminum-waste with acoustic properties. Waste Manag 2019;95:504–15. https://doi.org/10.1016/j.wasman.2019.06.042.
[38] Voronina NN, Horoshenkov KV. A new empirical model for the acoustic properties of loose granular media. Appl Acoust 2003;64:415–32. https://doi.org/10.1016/S0003-682X(02)00105-6.
[39] Arenas C, Leiva C, Vilches LF, González Ganso JA. Approaching a methodology for the development of a multilayer sound absorbing device recycling coal bottom ash. Appl Acoust 2017;115:184–91. https://doi.org/10.1016/j.apacoust.2016.08.021.
[40] J.F. Allard N. Atalla Propagation of sound in porous media: modelling sound absorbing materials 2nd ed., 2009 John Wiley & Sons 10.1002/9780470747339.
[41] Wallah SE. Drying shrinkage of heat-cured fly ash-based geopolymer concrete. Mod Appl Sci 2009;3:14–20. https://doi.org/10.5539/mas.v3n12p14.
[42] V.K. Bupesh Raja, S. Venugopal, S. Kannan, P.D. Sonawwanay, S. Sujan, S. Jeyanthi, et al., Sound barrier behavior of geopolymer composite manufactured from industrial waste, Materials Today: Proceedings, (2023) (in press/volume-page data not retrievable due to source access limits). doi:10.1016/j.matpr.2023.07.155.
[43] Venegas R, Umnova O. Acoustical properties of double porosity granular materials. J Acoust Soc Am 2011;130:2765–76. https://doi.org/10.1121/1.3644915.
[44] Alves AR, Simões MF, Simões S, Gomes J. A review on the scale-up of high-shear wet granulation processes and the impact of process parameters. Particuology 2024;92:180–95. https://doi.org/10.1016/j.partic.2024.05.007.
[45] Luukkonen T, Heponiemi A, Runtti H, Pesonen J, Yliniemi J, Lassi U. Application of alkali-activated materials for water and wastewater treatment: a review. Rev

Environ Sci Bio/Technol 2019;18:271–97. https://doi.org/10.1007/s11157-019-09494-0.

[46] Rudić O, Ducman V, Malešev M, Radonjanin V, Draganić S, Šupić S, et al. Aggregates obtained by alkali activation of fly ash: the effect of granulation, pelletization methods and curing regimes. Materials 2019;12:776. https://doi.org/10.3390/ma12050776.

[47] Kursula K, Mistri A, Illikainen M, Perumal P. Utilization of fine concrete waste as a lightweight aggregate via granulation: technical and environmental assessment. J Clean Prod 2024;434:139938. https://doi.org/10.1016/j.jclepro.2023.139938.

[48] Luukkonen T, Yu Y, Adhikary SK, Kauppinen S, Finnilä M, Perumal P. Metallic aluminium in municipal solid waste incineration fly ash as a blowing agent for porous alkali-activated granules. R Soc Open Sci 2024;11:240598. https://doi.org/10.1098/rsos.240598.

[49] Zolanvari SMH, Karlstetter C. In: Development of consolidated granular materials as sound absorbers: acoustical and mechanical characteristics. Berlin, Germany: German Acoustical Society (DEGA); 2013. p. 1768–71.

[50] UNE-EN 1936:2006, Natural stone test methods – Determination of real density and apparent density, and of total and open porosity, European Committee for Standardization (CEN), Brussels, Belgium, 2006.

[51] Rouquerol J, Llewellyn P, Rouquerol F. Is the BET equation applicable to microporous adsorbents? Stud Surf Sci Catal 2007;160:49–56. https://doi.org/10.1016/S0167-2991(07)80008-5.

[52] Sing K. The use of nitrogen adsorption for the characterisation of porous materials. Colloids Surf A Physicochem Eng Asp 2001;187–188:3–9. https://doi.org/10.1016/S0927-7757(01)00612-4.

[53] Dasgupta D, Nandi AK. Multiporosity in dried poly(vinylidene fluoride)–camphor systems: effect of drying method on porosity. Macromolecules 2007;40:2547–55. https://doi.org/10.1021/ma062709h.

[54] Iso. 10534-2, Acoustics — determination of sound absorption coefficient and impedance in impedance tubes — part 2: transfer-function method. Geneva, Switzerland: International Organization for Standardization; 2001. Accessed 13 February 2026.

[55] Owens ET, Daniels KE. Sound propagation and force chains in granular materials. EPL 2011;94:54005. https://doi.org/10.1209/0295-5075/94/54005.

[56] Liu CH, Nagel SR. Sound in a granular material: disorder and nonlinearity. Phys Rev B 1993;48:15646–50. https://doi.org/10.1103/PhysRevB.48.15646.

[57] Arenas JP, Crocker MJ. Recent trends in porous sound-absorbing materials. Accessed 15 February 2026 Sound & Vibration 2010;44:12–7. https://www.sandv.com.

[58] Ramlee NA, Jawaid M, Zainudin ES, Yamani SAK, Alamery S, Fouad H, et al. Thermal and acoustic properties of silane and hydrogen peroxide treated oil palm/bagasse fiber based biophenolic hybrid composites. Polym Compos 2022;43:3277–90. https://doi.org/10.1002/pc.26871.

[59] Alves C, Pelisser F, Labrincha J, Novais R. Effect of hydrogen peroxide on the thermal and mechanical properties of lightweight geopolymer mortar panels. Minerals 2023;13:542. https://doi.org/10.3390/min13040542.

[60] Gonzalez Rodriguez P, De Ruiter M, Wijnands T, Ten Elshof JE. Porous layered double hydroxides synthesized using oxygen generated by decomposition of hydrogen peroxide. Sci Rep 2017;7:2839. https://doi.org/10.1038/s41598-017-00283-9.

[61] Suo H, Xu J, Feng Y, Liu D, Tang P, Feng Y. Experimental research and theoretical analysis of the coupling mechanism between microstructure and acoustics in porous materials. Appl Sci 2025;15:3104. https://doi.org/10.3390/app15063104.

[62] Zhang S, Zou C, Peng C, Yan L, Wu X. Pore structure and its effect on acoustic velocity and permeability of reef-shoal carbonates in the Tarim Basin, Northwest China. J Geophys Eng 2022;19:1189–202. https://doi.org/10.1093/jge/gxac087.

[63] Xiong J, Liu J, Lin W, Li Y, Liao L, Wen M, et al. Enhanced broadband acoustic absorption in commercial foam via multiwall carbon nanotube-induced pore reconstruction. Adv Sci 2025:e202501898. https://doi.org/10.1002/advs.202501898.

[64] Thommes M, Kaneko K, Neimark AV, Olivier JP, Rodriguez-Reinoso F, Rouquerol J, et al. Physisorption of gases, with special reference to the evaluation of surface area and pore size distribution (IUPAC technical report). Pure Appl Chem 2015;87:1051–69. https://doi.org/10.1515/pac-2014-1117.

[65] Shi J, Liu B, Liu Y, Wang E, He Z, Xu H, et al. Preparation and characterization of lightweight aggregate foamed geopolymer concretes aerated using hydrogen peroxide. Constr Build Mater 2020;256:119442. https://doi.org/10.1016/j.conbuildmat.2020.119442.

[66] Park SB, Seo DS, Lee J. Studies on the sound absorption characteristics of porous concrete based on the content of recycled aggregate and target void ratio. Cem Concr Res 2005;35:1847–54. https://doi.org/10.1016/j.cemconres.2004.12.009.

[67] Bailhache S, Maillard J, Guigou-Carter C. Towards an alternative representation of indoor acoustic environment. Acta Acust 2022;6:45. https://doi.org/10.1051/aacus/2022045.

[68] Papa E, Medri V, Kpogbemabou D, Morinière V, Laumonier J, Vaccari A, et al. Porosity and insulating properties of silica-fume based foams. Energ Buildings 2016;131:41–9. https://doi.org/10.1016/j.enbuild.2016.09.031.

[69] T.J. Cox P. D'Antonio Acoustic absorbers and diffusers: theory, design and application 3rd ed., 2016 CRC Press 10.1201/9781315369211.

[70] Razumov DD. Models of acoustic resonators in studies of sound-absorbing structures. Microsystems, Electronics and Acoustics 2024;29:242–64. https://doi.org/10.20535/2523-4455.mea.314535.

[71] Zhou B, Zhang J, Li X, Liu B. An investigation on the sound absorption performance of granular molecular sieves under room temperature and pressure. Materials 2020;13:1936. https://doi.org/10.3390/ma13081936.

[72] Cox TJ, D'Antonio P. Book review: acoustic absorbers and diffusers: theory, design and application. Build Acoust 2005;12:255–8. https://doi.org/10.1260/135101005775219076.

[73] García-Cobos FJ, Maderuelo-Sanz R. Prediction of sound absorption performance of fibers coming from cigarette butts using a phenomenological model. J Ind Text 2022;51:1090S–S1112. https://doi.org/10.1177/15280837221097275.

[74] Iso. Acoustics — measurement of sound absorption in a reverberation room, International Organization for Standardization (ISO) 2003;354::2003. Accessed 13 February 2026.

[75] Bolt RH. Normal frequency spacing statistics. J Acoust Soc Am 1947;19:193–7. https://doi.org/10.1121/1.1916406.

[76] Han L, Wang J, Liu Z, Zhang Y, Jin Y, Li J, et al. Synthesis of fly ash-based self-supported zeolites foam geopolymer via saturated steam treatment. J Hazard Mater 2020;393:122468. https://doi.org/10.1016/j.jhazmat.2020.122468.

[77] Riyap AA, Bewa CN, Banenzoué C, Tchakouté HK, Rüscher CH, Kamseu E, et al. Microstructure and mechanical, physical and structural properties of sustainable lightweight metakaolin-based geopolymer cements and mortars employing rice husk. J Asian Ceram Soc 2019;7:199–209. https://doi.org/10.1080/21870764.2019.1606140.

[78] Le VS, Szczypinski MM, Hájková P, Kovacic V, Bakalova T, Volesky L, et al. Mechanical properties of geopolymer foam at high temperature. Sci Eng Compos Mater 2020;27:71–80. https://doi.org/10.1515/secm-2020-0013.

[79] Liu MYJ, Alengaram UJ, Jumaat MZ, Mo KH. Evaluation of thermal conductivity, mechanical and transport properties of lightweight aggregate foamed geopolymer concrete. Energ Buildings 2014;72:238–45. https://doi.org/10.1016/j.enbuild.2013.12.029.

[80] Shen L, Luo Y, Ni L, Liang M, Zhou S, Zou H. Constructing hierarchical pore structures in melamine foams with silver and cellulose nanofiber to achieve broadband sound absorption and enhanced mechanical performance. Carbohydr Polym 2025;355:123344. https://doi.org/10.1016/j.carbpol.2025.123344.

[81] Schäfer K, Nestler D, Kroll L. Impact compressive properties of polyurethane foams with 3D continuous fibre reinforcement. Proceedings of the Institution of Mechanical Engineers, Part L: Journal of Materials: Design and Applications 2025;239:706–19. https://doi.org/10.1177/14644207241304639.

[82] Jaouen L, Renault A, Deverge M. Elastic and damping characterizations of acoustical porous materials: available experimental methods and applications to a melamine foam. Appl Acoust 2008;69:1129–40. https://doi.org/10.1016/j.apacoust.2007.11.008.

[83] Zaragoza-Benzal A, Formosa J, Chimenos JM. Recovery of End-of-Life Tyres and Mineral Wool Waste: a Case Study with Gypsum Composite Materials applying Circular Economy Criteria. Materials 2023;16:243. https://doi.org/10.3390/ma16010243.

[84] Guna V, Ilangovan M, Hu M. Wool and coir fiber reinforced gypsum ceiling tiles for building applications. Journal of Building Engineering 2021;44:102433. https://doi.org/10.1016/j.jobe.2021.102433.

[85] Kim KW, Jeong JH, Lee JS. Deflection of resilient materials for reduction of floor impact sound. Appl Sci 2014;2014:612608. https://doi.org/10.1155/2014/612608.

[86] Mahmoud HA, Tawfik TA, Abd El-razik MM, Faried AS. Mechanical and acoustic absorption properties of lightweight fly ash/slag-based geopolymer concrete with various aggregates. Ceram Int 2023;49:20131–42. https://doi.org/10.1016/j.ceramint.2023.03.244.

[87] Acoustic Group, Absorption coefficients for building materials, https://www.acoustic.ua/st/web_absorption_data_eng.pdf (Accessed 13 February 2026).